DC Wind Turbine Circuit with Series-Resonant DC/DC Converter

Mario Zaja

Supervisor: Philip Carne Kjær

AALBORG UNIVERSITY
DENMARK

Acknowledgements

I hereby thank everybody who helped me during the period of working on this thesis. I particularly thank my supervisor Philip Carne Kjær, PhD student Catalin Gabriel Dincan and lab supervisor Walter Neumayr for all the assistance provided. I would also like to thank all my university colleagues, the whole Energy Technology Department, Vestas Wind Systems with all my co-workers there and Aalborg University in general. Special thanks goes to my friends and family for supporting me during my stay here.

Contents

1 Abstract

Offshore wind farms are connected to land by HVDC cables, with voltage source converters placed at both ends. The power output of each turbine is collected as AC at a medium voltage level, meaning that each turbine has to contain an AC-DC-AC converter. A promising approach to reduce the size of related power conversion equipment and conversion losses is to make each of the turbines output power as DC at a medium voltage level, which can then be collected and stepped up at a HVDC platform. The turbine DC-AC converter could be replaced by a series-resonant DC-DC converter using a medium-frequency transformer to step up the voltage. The main benefit of operating in a higher frequency range is the reduction in size and weight of the equipment used. However, the new approach also brings additional challenges, such as the relatively narrow operating range of such a converter and high voltage and current stress on its components. This document contains theoretical analysis of such a circuit, component selection, control system design and circuit validation, both by simulation and a downscale hardware setup.

2 Summary

This document is a 10th semester Master Thesis of the Master program in Power Electronics and Drives at Aalborg University, made in collaboration with Vestas Wind Systems A/S. For easier readability, the contents of each section have been briefly summarized.

Introduction contains general motivation for the project, project scope and goal, problem definition and a brief description of the development procedure.

DC-DC series-resonant converter circuit section contains in depth analysis of the converter topology and its electrical properties, obtained both analytically and using simulation software. The section analyzes the impact of various design variables on the circuit's behavior and gives general converter design guidelines.

Resonant converter design contains a 10 MW circuit proposal based on the findings of the previous section, including a corresponding control system and auxiliary circuits.

Model validation contains a description of the downscale lab prototype setup, loss estimation of the same circuit made in Plecs and a comparison between the waveforms obtained in simulation and on an actual setup.

Conclusion contains an overview of the most important points stated in the report.

List of abbreviations contains an explanation of all the abbreviations used in the report.

References section contains a list of all the external sources used in the report.

Appendix contains a list of supplementary contents available on the attached CD, including the developed analysis tool, simulation models, plot catalogue and device datasheets.

The most important findings of main chapters (4, 5 and 6) have been additionally summarized at the end of each chapter to make it easier to follow the report.

3 Introduction

Offshore wind power is at the moment the most competitive renewable energy source [1] and therefore under a great focus over the last several years. Compared to on-shore wind power technologies, offshore solutions feature a lower levelized cost of energy and a lot higher power output per turbine, which can reach up to 10 MW at the present day. Handling those great amounts of energy presents many new challenges, and the initiative to reduce the costs even further and increase competitiveness is very strong.

The state-of-the-art offshore wind farm is shown in Figure 1. Wind turbines are connected to a MVAC bus leading to the platform containing the HV transformer. The output power of the HV transformer is transferred through the HVAC cable to a rectifier station on another platform, where AC-DC conversion is made. Finally, the power of the whole wind park is transferred to the shore via a HVDC cable, where another DC-AC conversion is performed and grid connection established.

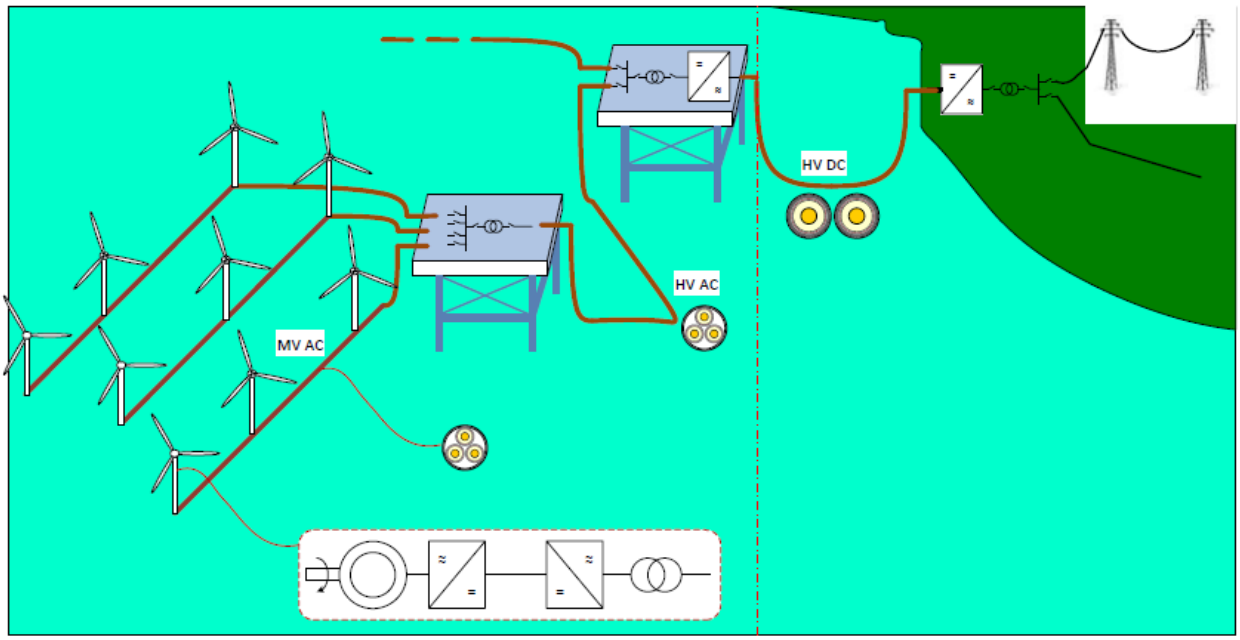

Figure 1 - State-of-the-art offshore wind farm

There are several downsides of this approach. First, to be able to connect to the MVAC bus, each of the turbine has to have its own AC-DC-AC converter and a MV transformer. Second, the HV transformer substation operates at a 50/60 Hz frequency and needs to be able

to handle the total power output from all the MVAC busses connected to it, meaning that it will be large and heavy and therefore require a separate platform to support it. Reliability is also an issue since a fault on the HV transformer would bring the power production from all the turbines connected to it to a halt. Finally, another large transformer is required on the second platform containing the AC-DC converter, having the same issues as previously discussed. The power is converter several times before reaching the shore, resulting in significant conversion losses.

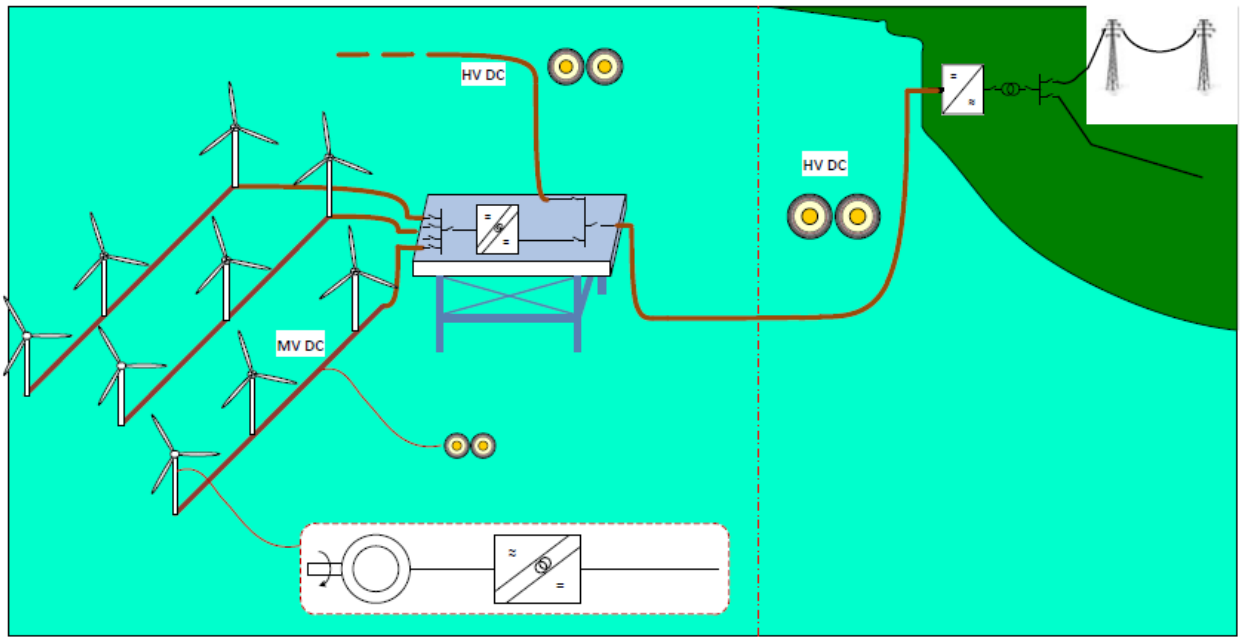

Figure 2 - The proposed offshore wind farm layout

The proposed wind farm solution is shown in Figure 2. Here, the line DC-AC inverter and a HV transformer have been replaced by a DC-DC converter using a MF transformer. The output of all turbines is collected as MVDC and connected to a DC-DC substation for stepping up the voltage and transferring it to the shore via a HVDC cable. The main benefit of this approach is performing the LVDC/MVDC conversion at a much higher frequency, resulting in significant reduction of the equipment's size and weight, which can now be stored in each of the turbines. As a consequence, this approach completely eliminates the need for an offshore platform carrying the HV transformer, significantly reducing the costs and improving reliability.

3.1 Goal, problem definition and methodology

The goal of this project is to analyze, design and validate a series-resonant DC-DC converter circuit, as well as its corresponding control system. 10 MW and 150 W circuit proposals will be made, of which the latter will be used to experimentally validate the results.

There are several challenges to overcome in the circuit design process:

- The resonant tank's response is nonlinear to the change of driving signal's frequency
- The circuit's response sensitivity increases as the frequency approaches its resonant value, which might render the system unstable
- The resonant tank components are subject to very high voltage and current stress even during normal operation
- The additional components, such as the medium-frequency transformer or the smoothening capacitors, can have a significant impact on the circuit's frequency response

Circuit analysis and control system design tasks will be performed both analytically and using computer simulation tools Plecs and Matlab. The purpose of experimental verification will be to evaluate the voltage and current waveforms obtained by lab prototype simulation. Experimental verification will be carried out on a real hardware setup containing a full bridge converter, resonant tank, medium frequency transformer, passive rectifier and a signal generator to manually control the circuit in open loop.

4 DC-DC series-resonant converter circuit

4.1 Equivalent circuit model

A principal series-resonant DC-DC converter (SRC) circuit is shown in Figure 3.

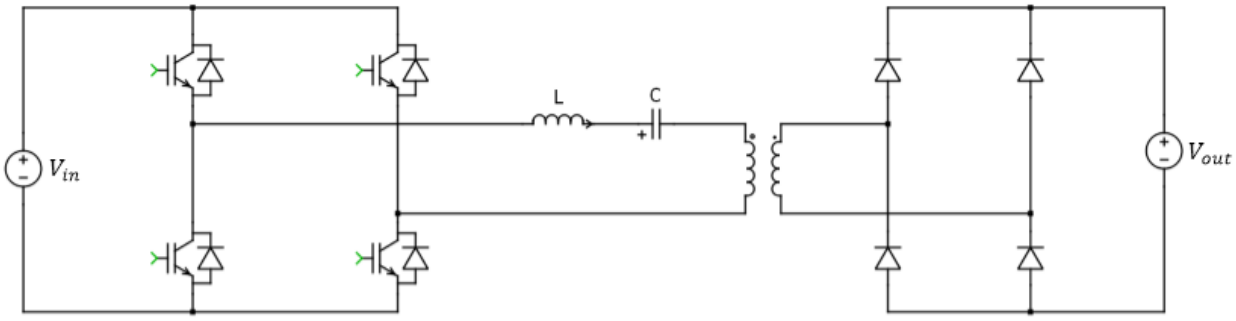

Figure 3 - Simple DC-DC series-resonant converter schematic

The circuit consists of a controllable full bridge converter, a resonant LC tank, a MF transformer and a passive full bridge diode rectifier. To simplify the analysis, it will be assumed that both of the converter terminals have ideal voltage sources connected to them, meaning they provide constant load voltage independent of the current. The MF transformer is ideal with a transfer ratio of 1:1. Resonant tank components are also ideal, being purely reactive and having no saturation. Finally, the power converter and diode rectifier are ideal as well, switching instantaneously and having no losses.

The circuit is controlled by giving a set of pulses to the converter and producing a square wave voltage at its output. The resonant tank rings with the frequency of the square wave, producing an AC current. The current passes through the transformer windings, creating an alternating magnetic field and thus inducing the voltage on the secondary side. Finally, the secondary AC current produced is rectified in the passive diode rectifier and fed into the active load.

The input voltage waveform is a square wave with either positive or negative value of the magnitude of the input voltage. Assuming the square wave is symmetrical, its spectrum is given by

$$v_s(t) = \frac{4\,V_{in}}{\pi} \sum_{n=1,3,5\ldots} \frac{1}{n} \sin(2n\pi f_s t) \tag{1}$$

Where V_{in} is the input voltage and f_s the frequency of the square wave. Ideal resonant tank's admittance can be expressed as

$$Y_{tank} = \frac{sC}{s^2LC + 1} \tag{2}$$

The Bode diagram of a generic resonant tank's admittance described by (2) is shown in Figure 4.

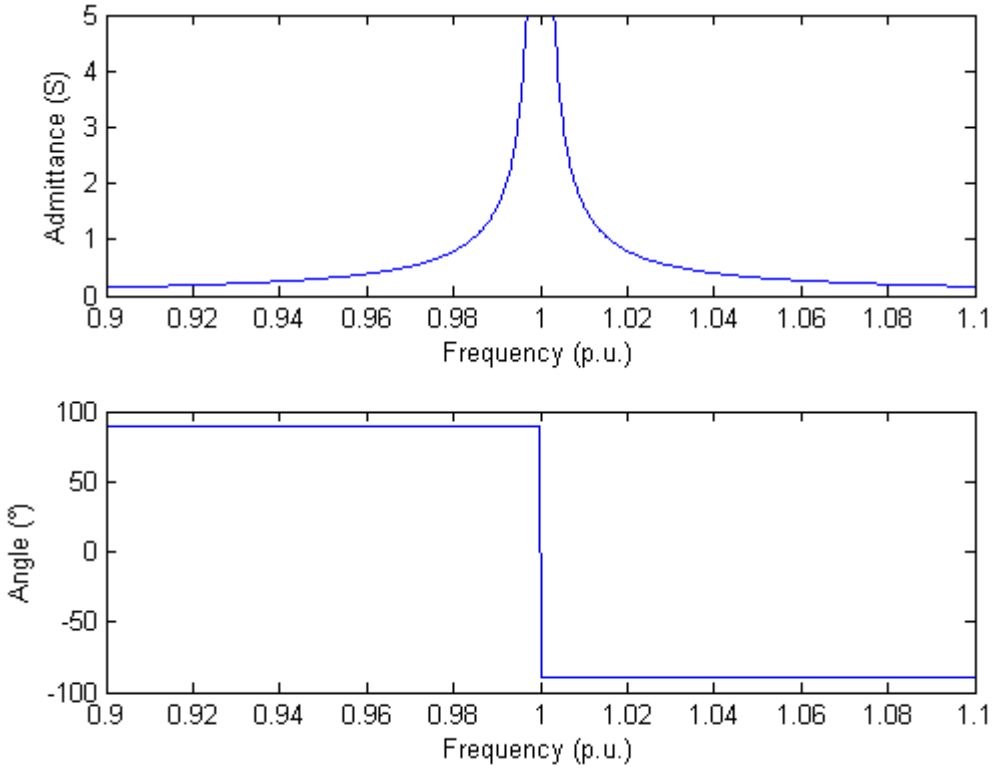

Figure 4 - Bode diagram of a generic resonant tank

From the amplitude plot it is visible that the resonant tank acts like a narrow band pass filter. This means that the resonant tank only responds to the fundamental component while all the higher order harmonics from (1) are attenuated and have no practical impact on the resonant tank current. Therefore the converter's output terminal can be modelled as an ideal sinusoidal voltage source with

$$v_s(t) = \frac{4\,V_{in}}{\pi}\sin(2\pi f_s t) \tag{3}$$

The frequency at which the resonant tank's admittance becomes infinite, also shown as 1 p.u. on the Bode plot, is called the resonant frequency and can be calculated as

$$f_{res} = \frac{1}{2\pi\sqrt{LC}} \tag{4}$$

As visible from the Bode plot, the band pass region gain is virtually symmetrical around the resonant frequency, but the phase changes from +90° to -90°. This means that in the sub-resonant region the tank performs capacitive, while in the super-resonant region it becomes inductive. This also demonstrates the basic control principle of resonant conversion – the admittance, and therefore the amplitude of the AC current, can be controlled by adjusting the square wave frequency around the resonance region.

As stated before, the current through the resonant tank can be viewed as pure sinusoidal. This current will have a certain phase offset φ_s with respect to the converter output voltage, which can be expressed as

$$i_s(t) = \hat{I}_s \sin(2\pi f_s t + \varphi_s) \tag{5}$$

φ_s can be both positive and negative, depending on whether the converter operates in the capacitive or the inductive mode. If the switching frequency equals the resonant frequency, $\varphi_s = 0$.

The current waveform drawn by the converter is shown in Figure 5.

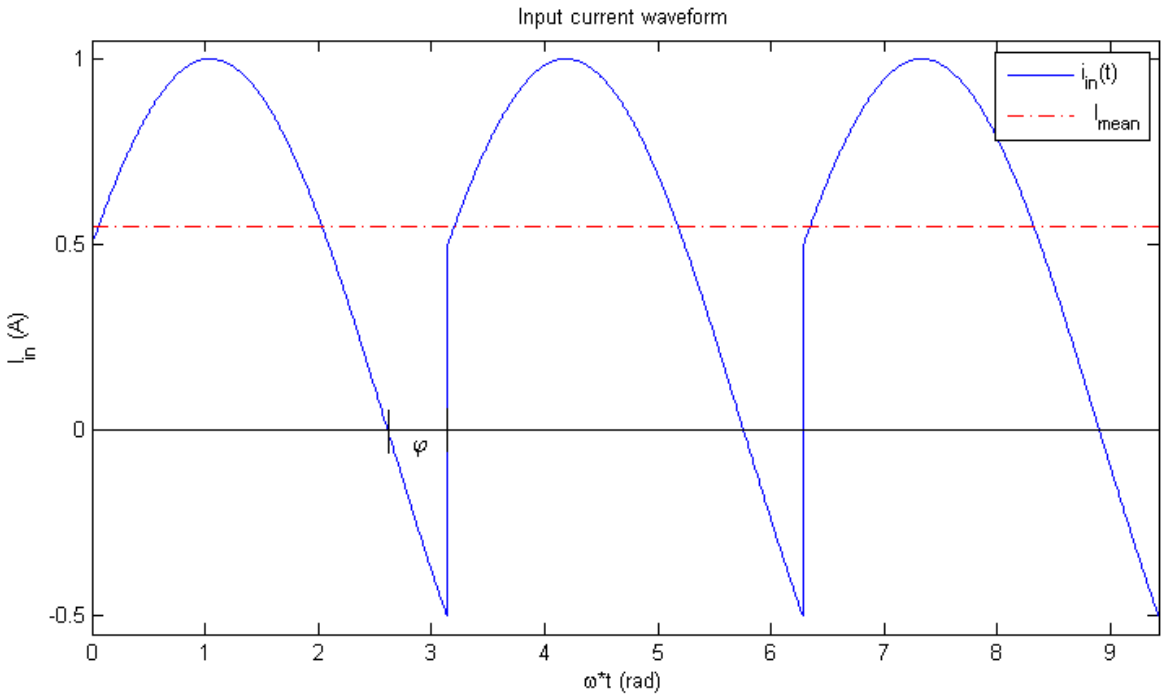

Figure 5 - Input current waveform and its mean value

Averaging the current over one switching period gives

$$\langle i_{in}(t)\rangle_{T_s} = \frac{2}{\pi}\,\hat{I}_s\cos(\varphi_s) \tag{6}$$

Therefore, the input port of the switch network can be modelled as a DC current source as described by (6).

The voltage at the rectifier's input port is determined by the resonant tank current. As the load is an ideal DC voltage source, the voltage at the rectifier's input port is a square wave in phase with the resonant tank current. However, since the resonant tank responds only to the fundamental component, the rectifier's input port can also be modelled as a sinusoidal voltage source.

$$v_r(t) = \frac{4\,V_{out}}{\pi}\,\sin(2\pi f_s t + \varphi_s) \tag{7}$$

Finally, the full bridge diode rectifier outputs a rectified sinusoidal current waveform to the active DC load. The average current value over one switching period is calculated as

$$\langle i_{out}(t)\rangle_{T_s} = \frac{2}{\pi}\,\hat{I}_s \tag{8}$$

Using the results from (3), (6) - (8), an equivalent series-resonant converter circuit can be constructed. The result is shown in Figure 6.

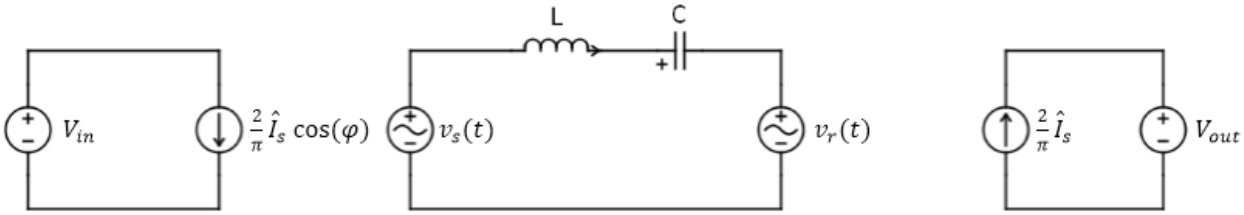

Figure 6 - Equivalent electrical circuit of a series-resonant DC-DC converter

4.2 Steady-state analysis

This section analyzes the natural response of an ideal DC-DC converter circuit depicted in Figure 3. All the earlier mentioned limitations still apply. The resonant tank elements had been chosen according to two criteria – to have the resonant frequency of 5000 Hz and characteristic impedance of 1 Ω. The characteristic impedance is given by

$$Z_{LC} = \sqrt{\frac{L}{C}} \tag{9}$$

In other words, the L and C values had been chosen in such a way that $L = C$. This was done for no other reason but to simply the per-unit analysis. The full list of per-unit base values is given in Table 1.

Table 1 - List of base values for per-unit analysis

Base unit	Base unit value
V_{base}	1 V
P_{base}	10 W
I_{base}	10 A
f_{base}	5000 Hz
L_{base}	31.831 µH
C_{base}	31.831 µF

In all of the simulation runs, the output, inductor, IGBT and diode currents and capacitor voltage waveforms had been captured and analyzed. However, due to limited amount of space in the report, only several selected plots have been shown. The full plot catalogue is located on the attached CD.

4.2.1 Input and output voltage

The first set of figures depicts how the monitored quantities change as the input and output voltages change. This analysis is important as the actual voltages on both ends of the converter will change during normal operation, typically within range of ± 10%. In this simulation set, the switching frequency was kept constant at 0.96 p.u. with a duty cycle of 1. Each point is evaluated at the steady state.

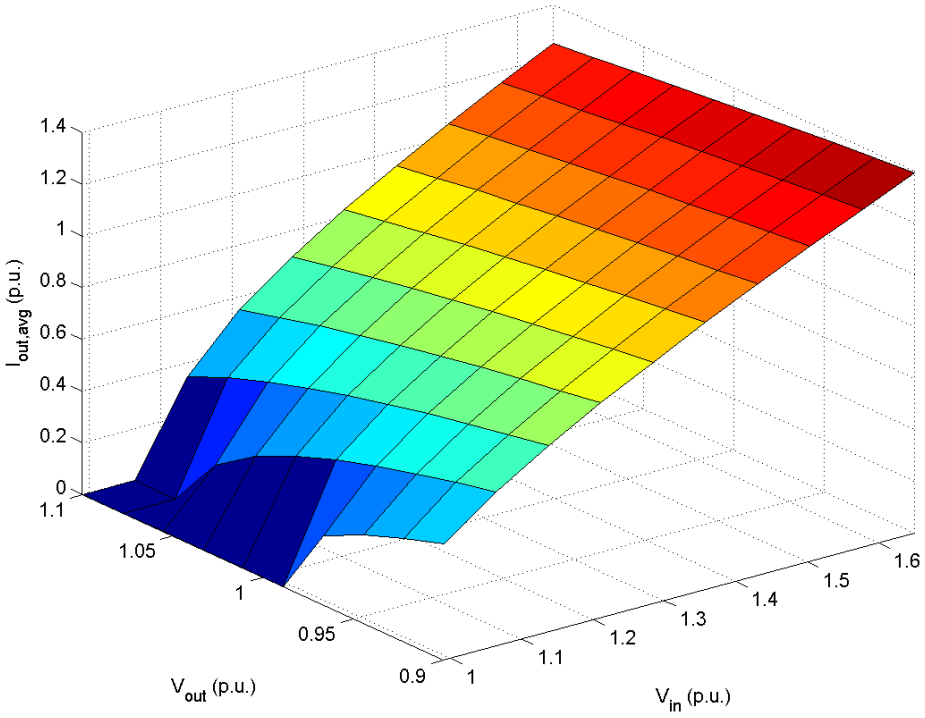

Figure 7 - Output current dependence on input and output voltage changes

The dark blue region in Figure 7 shows the case when the output voltage is above the input voltage. As the output side of the converter is connected through a full bridge diode rectifier, the current, and thus the power, can only flow in one direction, from the input to the output. The boundary condition for this state is

$$V_{in} = V_{out} \tag{10}$$

For all the values where

$$V_{in} \leq V_{out} \tag{11}$$

, all the rectifier diodes are reverse-biased and thus the converter is inoperable. Therefore, the necessary condition for normal converter operation is given by

$$V_{in} > V_{out} \tag{12}$$

It is of highest importance in the resonant converter design that (12) is valid at all times. This property will therefore directly influence the choice of the transformer transfer ratio. For this purpose it is useful to define the DC voltage transfer ratio as

$$k_v = \frac{V_{in}}{V_{out}} \tag{13}$$

Analyzing the results further, it is visible that the relationship between the voltage transfer ratio and output current is not linear. This property is more clearly displayed in Figure 8.

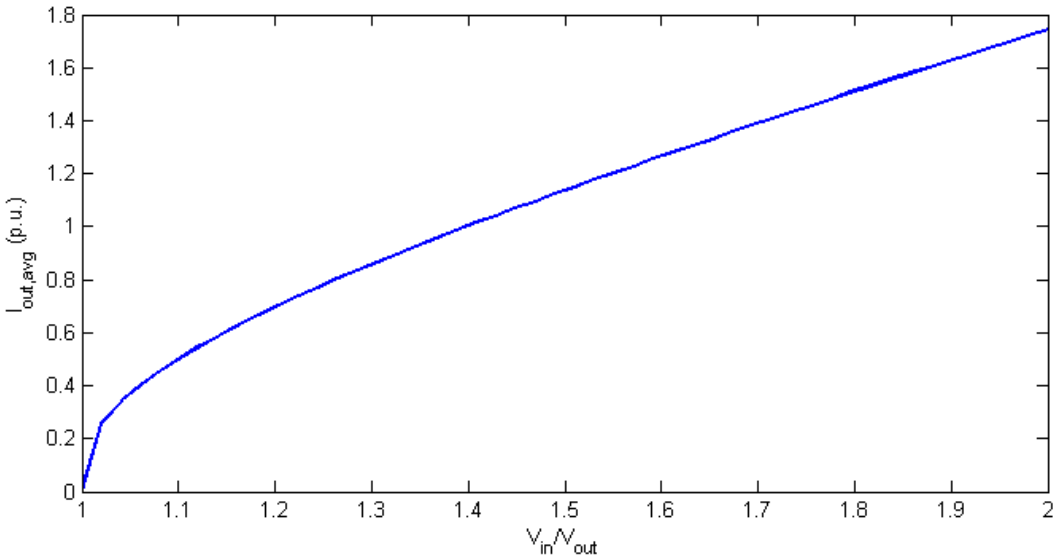

Figure 8 - Relationship between the voltage transfer ratio and the average output current

In the region where $k_v \approx 1$, the dependence between the voltage transfer ratio and the output current value is strongly nonlinear, putting additional requirements on the control

system design. Drifting further away from the boundary region, the relationship becomes more and more linear.

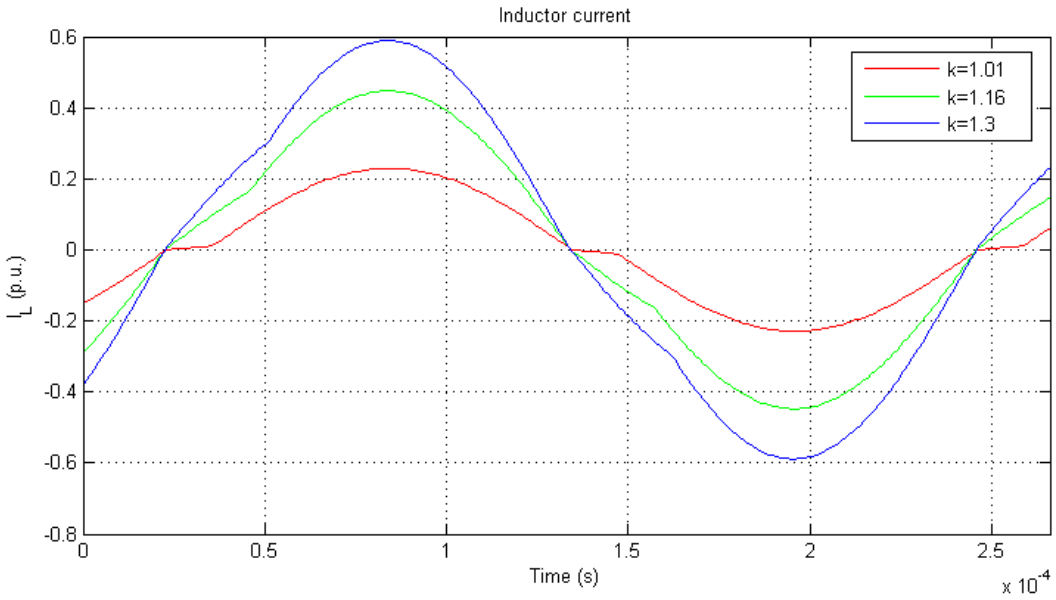

Figure 9 - Inductor current waveforms for different values of the voltage transfer ratio

The reason for this nonlinear behavior is shown in Figure 9. When the factor k_v is sufficiently small, the converter enters discontinuous conduction mode (DCM), as represented by the red line. The figure also shows that the actual current waveforms are not purely sinusoidal even in the continuous conduction mode (CCM). However, as the voltage transfer ratio increases, the inductor current resembles the pure sine wave more and more closely.

4.2.2 Input voltage and switching frequency

This simulation set shows how altering the input voltage and switching frequency affects the circuit's behavior. The output voltage was kept constant at 1 p.u., which means that the V_{in} value can also be interpreted as k_v. The rest of the parameters were the same as in the previous simulation runs.

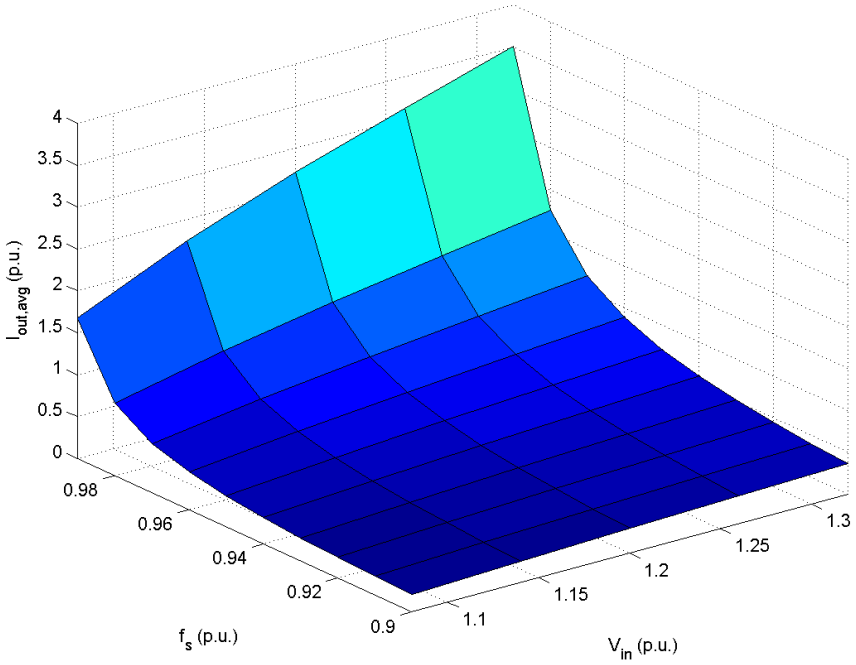

Figure 10 - Output current dependence on input voltage and switching frequency changes

Overall, the frequency was varied from 0.9 to 0.99 p.u. As already mentioned and shown in the Bode plot in Figure 4, the resonant tank's admittance is a function of the applied signal's frequency and that is the key property used to control the resonant power converters. As the signal's frequency gets closer to the resonant frequency, the slope of the curve gets steeper. For an ideal, lossless circuit, the tank has infinite admittance at the resonant frequency.

The theoretical model corresponds well with the obtained simulation results, as shown in Figure 10. For a constant voltage transfer ratio, the output current magnitude is proportional to the tank's admittance. The shape of the curves describing the change of the output current magnitude along the lines of a constant voltage transfer ratio can be described by a rational function as

$$y = \left| \frac{a_1 x}{1 - a_2 x^2} \right| \tag{14}$$

, where a_1 and a_2 are arbitrary constants. This corresponds to the shape of the resonant tank's admittance curve depicted in Figure 4.

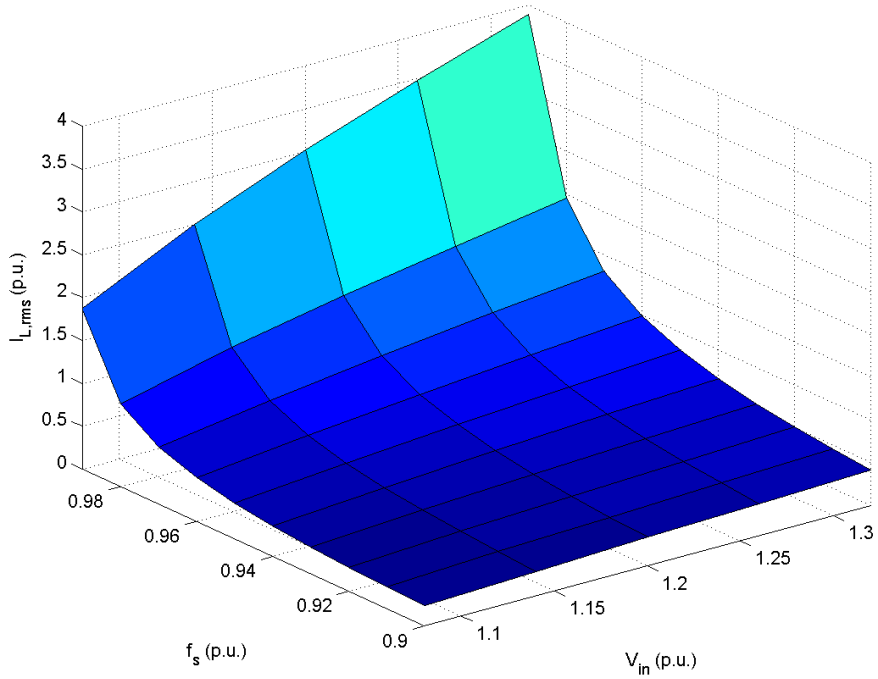

Figure 11 - Inductor current dependence on input voltage and switching frequency changes

The main property to be observed from Figure 11 and Figure 12 is a major increase in component stress when operating close to the resonance region. Since series topology is used, this increase is naturally proportional to the average output current, and thus the output power. Two of the key parameters to be considered in the resonant tank design process are the inductor current and capacitor voltage values in steady state. Overall, the voltage and current ratings of these two components will define the maximum power that can be transferred through the circuit.

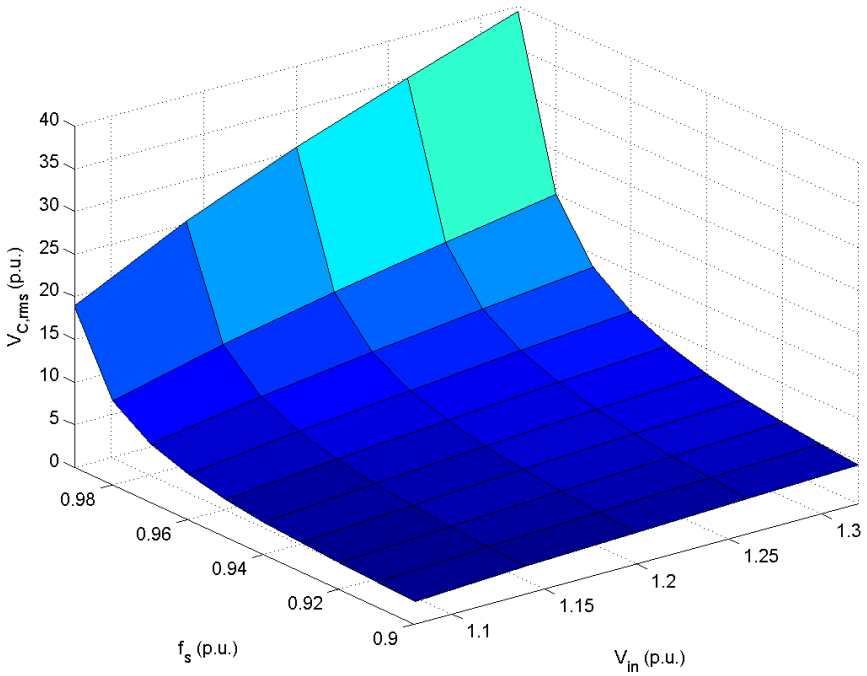

Figure 12 - Capacitor voltage dependence on LVDC voltage and switching frequency changes

The voltage stress of the components is particularly important to observe in this case. At the frequency of 0.9 p.u. and V_{in} value of 1.08, the RMS value of the capacitor voltage equals 2.65 p.u. At the same time, at the frequency of 0.99 p.u., the voltage value rises to 18.9 p.u., which is more than a sevenfold increase caused by a 10% frequency change. This clearly indicates two things. First, the resonant tank components will need to be rated to a lot higher voltage level than the turbine's DC output, meaning that their cost might be dominant in the overall price of the solution. This will likely impose many design restrictions on both the lab prototype and full scale solution. Second, sensitivity of the controller has to be very high to operate the circuit close to the resonant region. This means that all the measurement, quantization, discretization and all other types of numerical errors will have an increased impact on the control system and might cause overloading of the components. To prevent this from happening, several types of hard-stop protection will need to be implemented.

However, not only the increase in frequency significantly increases the voltage and current stress, but it also increases the circuit's sensitivity to voltage changes. This is more closely shown in Figure 13.

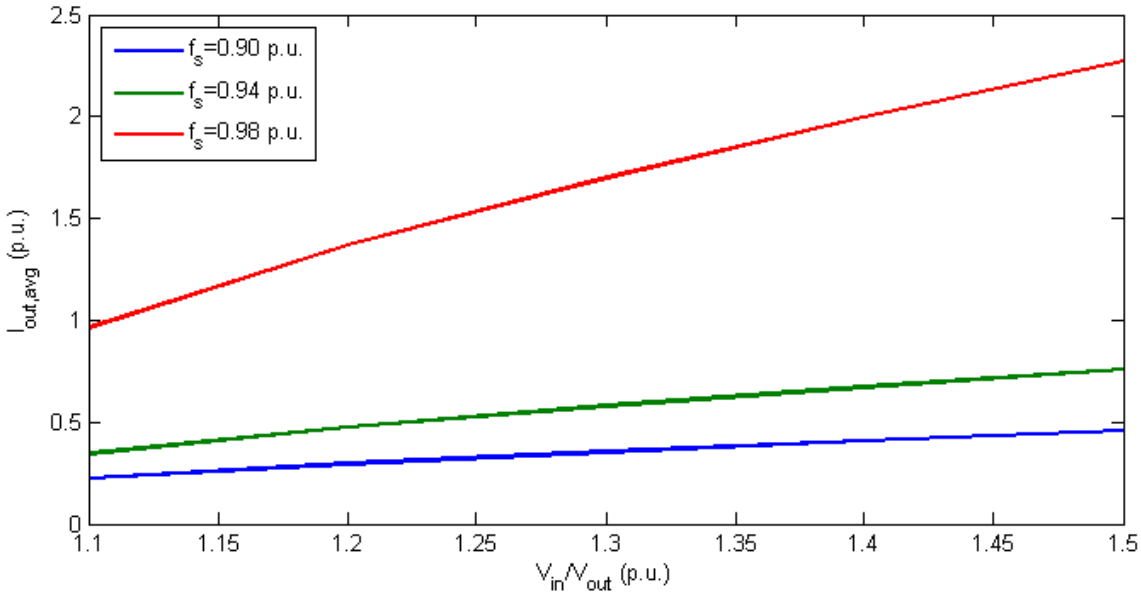

Figure 13 - The impact of voltage transfer ratio change at different switching frequencies

The closer the switching frequency to the resonant, the higher will the impact of the voltage transfer ratio change be, which is a natural consequence of increasing the resonant tank's admittance. This imposes new challenges on the circuit design, as the voltage transfer ratio will change unpredictably in the real converter, which could cause a sudden and uncontrolled surge in the component stress. Therefore, the worst case of a stress surge will need to be evaluated and maximum permissible switching frequency selected at which the components can still withstand it.

4.2.3 Output voltage and switching frequency

The circuit responds to a change in the output voltage in a similar manner as for the input, since those two values define the voltage transfer ratio k_v. Therefore this section does not contain any new information about the circuit's behavior and has been skipped. The simulation results can however be found on the attached CD.

4.2.4 Inductance and capacitance

The following set of figures shows how the selection of L and C values affects the circuit. The inductance was varied between 0.5 and 10 p.u., while the capacitance between 0.1 and 2 p.u. For each combination of L and C values a new resonant frequency was calculated. The

switching frequency in each of the test cases was chosen as 95% of the corresponding resonant frequency.

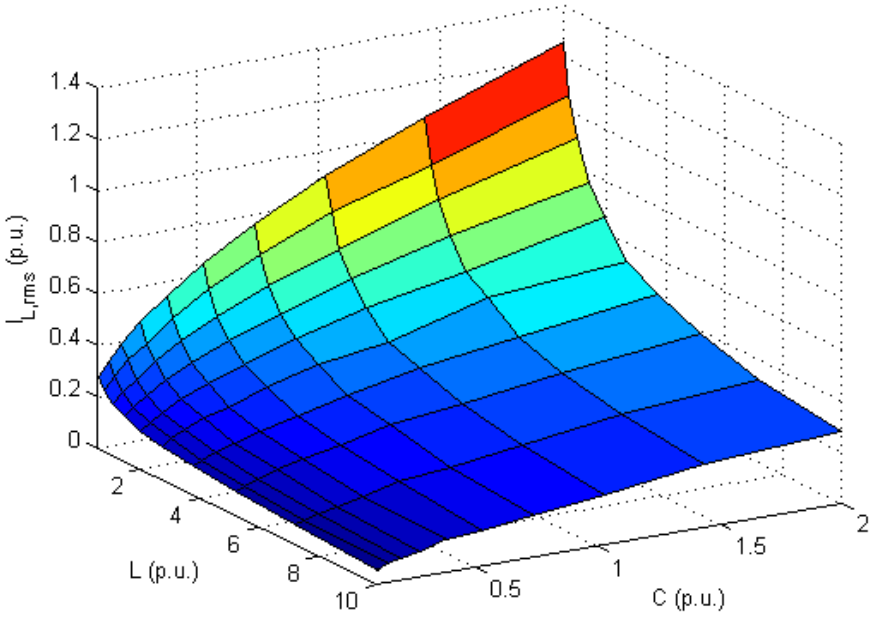

Figure 14 - The impact of L and C choice on the inductor current

The inductor, and thus the output current, rise with the increase of capacitance and decrease of inductance. This behavior can also be characterized analytically. The ratio between the switching and resonant frequency can be defined as

$$k_f = \frac{f_s}{f_{res}} = \frac{\omega_s}{\omega_{res}} \tag{15}$$

The inductor current corresponds to the product of a voltage drop across the resonant tank multiplied by its admittance. Assuming the circuit is in steady state and the waveforms are ideal sinusoidals, the tank's admittance is given by

$$Y_{tank} = \left| \frac{\omega C}{1 - \omega^2 LC} \right| \tag{16}$$

Combining (4) and (15) yields

$$\omega_s = \frac{k_f}{\sqrt{LC}} \tag{17}$$

Substituting the angular frequency from (16) with (17) and simplifying the expression gives

$$Y_{tank} = \left|\frac{k_f}{1-k_f^2}\right|\sqrt{\frac{C}{L}} \tag{18}$$

Equation (18) shows that the inductor current is proportional to the tank's characteristic admittance, which is the inverse value of its characteristic impedance defined in (9).

$$Y_{LC} = Z_{LC}^{-1} = \sqrt{\frac{C}{L}} \tag{19}$$

This means that, for the same relative value of the switching frequency, the tank's admittance will increase with the capacitance and decrease with the inductance value. The result obtained in (18) corresponds well with Figure 14.

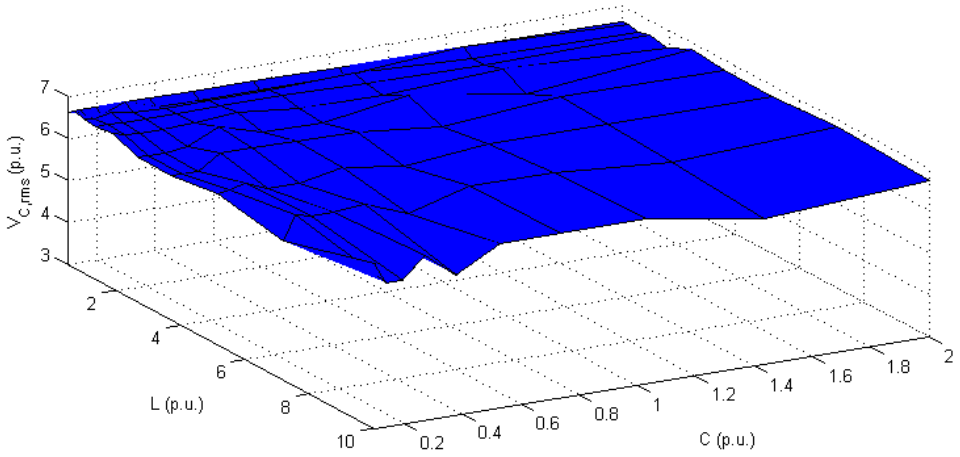

Figure 15 - The impact of L and C choice on the capacitor voltage

At the same time, Figure 15 shows that the capacitor voltage is independent of the choice of L and C. The capacitor voltage can be expressed using a simple voltage divider equation as

$$V_c = \frac{V_{tank}}{|1 - \omega^2 LC|} \tag{20}$$

Substituting the angular frequency in (20) with (17) and simplifying the expression yields

$$V_c = \frac{V_{tank}}{|1 - k_f^2|} \tag{21}$$

Equation (21) shows that the capacitor voltage is dependent only on the relative value of switching frequency and not the component selection. This corresponds to the results shown in Figure 15.

From this section's findings, several guidelines for the resonant tank design can be derived. The resonant frequency should be chosen first. Once the resonant frequency is selected, the nominal k_f factor can be calculated based on the desired capacitor voltage.

Assuming an ideal circuit as shown in Figure 6, the resonant tank's voltage drop can be calculated as a difference between the voltage at the converter´s output terminal and the voltage at the rectifier's input terminal. Since the resonant network is purely reactive and rectifier voltage is in phase with the tank current, these two voltages are shifted by 90°. The resonant tank voltage can therefore be calculated as

$$V_{tank} = \sqrt{V_s^2 - V_r^2} \tag{22}$$

Combining (21) and (22) and substituting V_s and V_r for known variables, peak capacitor voltage can be calculated as

$$\hat{V}_c = \frac{4}{\pi} \frac{\sqrt{V_{in}^2 - V_{out}^2}}{|1 - k_f^2|} \tag{23}$$

Using (23), the maximum desired k_f and therefore the switching frequency can be obtained. Once the switching frequency is chosen, the inductance value is selected to achieve

the desired tank's admittance and consequently the maximum power that can be transferred through the circuit. Since the rectifier is ideal, the power at its input terminal is the same as the power at its output. Moreover, as it operates as a purely resistive load, the output power can be expressed as

$$P_{out} = I_s V_r \tag{24}$$

The tank's current is a product of a voltage drop across the tank and its admittance. The voltage drop across the resonant tank is known from (22). Therefore, if the desired output power is known, the required tank's admittance can be calculated as

$$Y_{tank} = \frac{P_{out}}{\frac{2\sqrt{2}}{\pi} V_{out} \cdot \sqrt{V_{in}^2 - V_{out}^2}} \tag{25}$$

Once the desired admittance value has been obtained, the inductance value can be calculated. Since the resonant frequency is already known, the capacitance from (4) can be expressed as

$$C = \frac{1}{L\omega_{res}^2} \tag{26}$$

Combining (18) and (26), the desired tank's inductance can be calculated as

$$L = \left| \frac{k_f}{1 - k_f^2} \right| \frac{1}{Y_{tank}\, \omega_{res}} \tag{27}$$

Once the inductance value is chosen, the capacitance can finally be obtained using (26).

4.2.5 Frequency and duty cycle

This section shows how the circuit responds to an addition of dead time to the driving signal. The signal is shown in Figure 16.

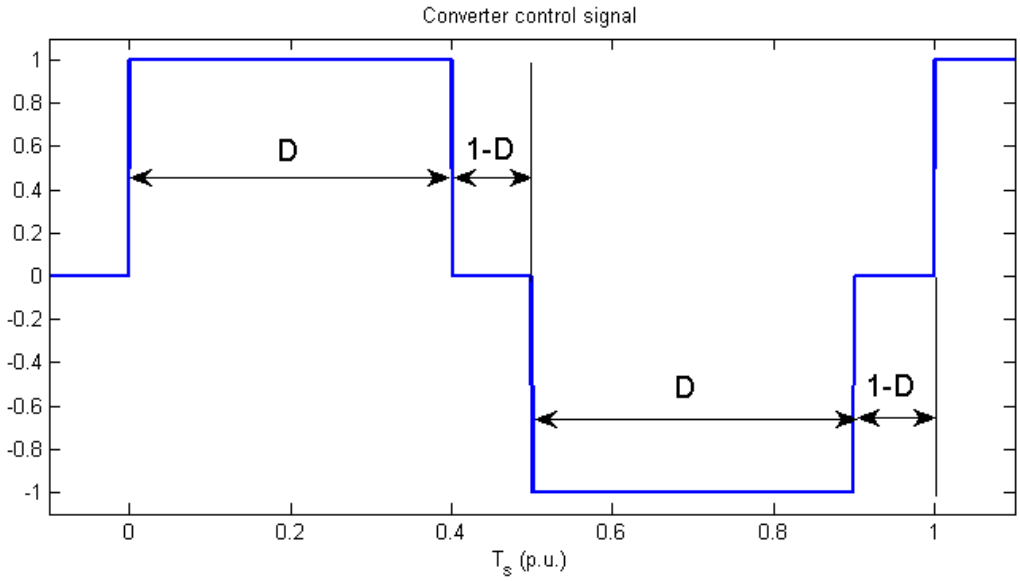

Figure 16 - Converter control signal with dead time

Figure 17 shows that, in case the dead time is between 0 and 15%, there is no practical impact on the circuit's performance. From 15-35%, the circuit's performance drops drastically, while for all the dead time values above 35% the circuit becomes practically inoperable. While the results show that there are no benefits in using dead time for circuit control, they also infer that the small dead time values present in real system will not affect the circuit's performance. This is a very positive property, especially from the control viewpoint.

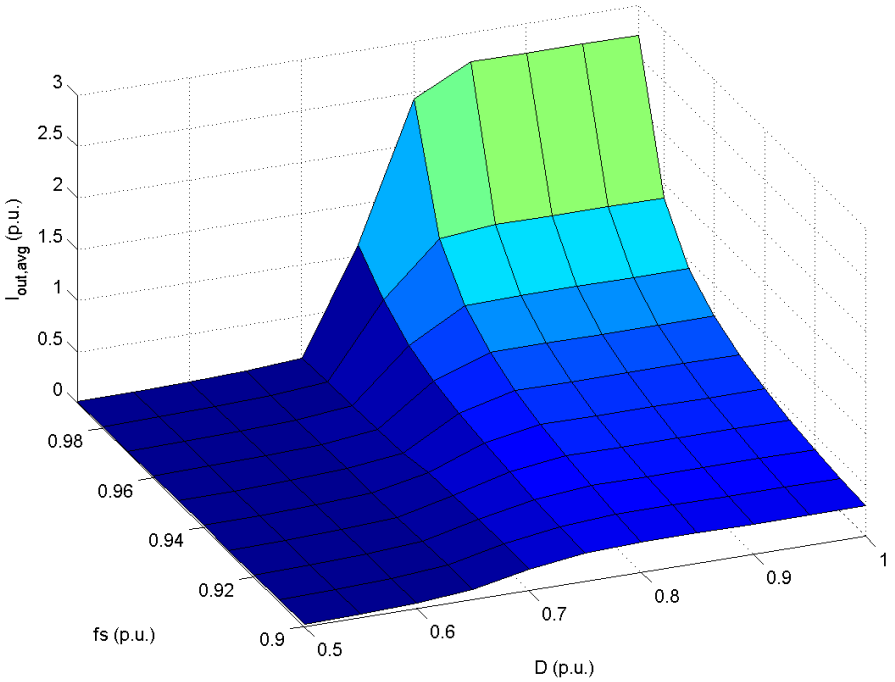

Figure 17 - The impact of dead time on output current

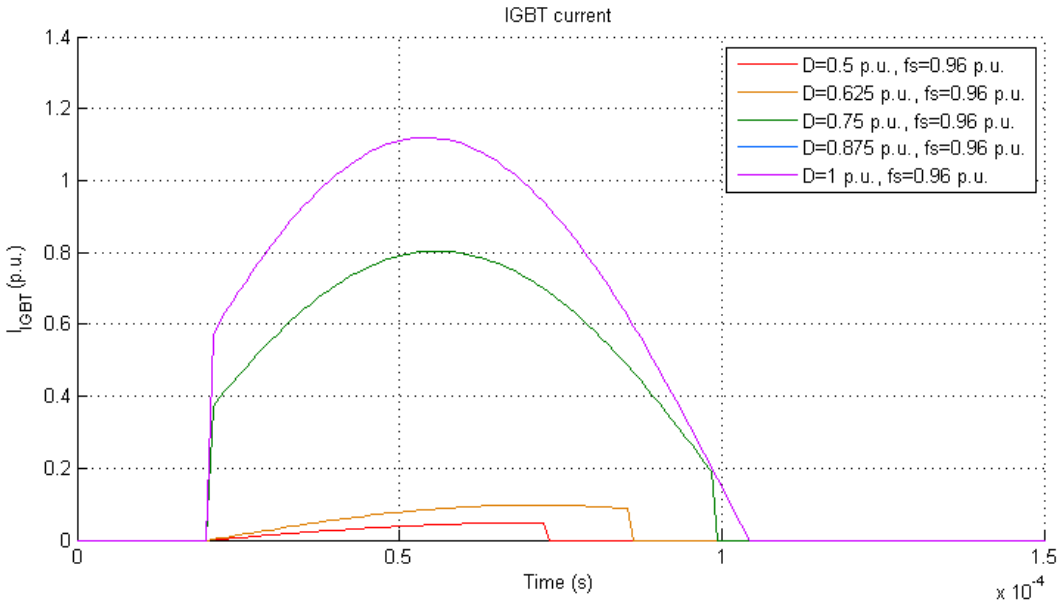

Figure 18 - IGBT current waveforms for different dead time values

Figure 18 shows the impact of dead time on transistor current. For small dead times, there is no practical impact as can be seen from the blue and the purple curve which are practically the same. However, as the dead time increases, the circuit eventually enters the discontinuous conduction mode.

The reason for such a behavior is the following - since there is not enough time for the current to decrease naturally to zero, the transistor gets turned off while still conducting. At the same time, the current cannot change instantaneously due to resonant tank's inductor and therefore retains its direction, forward-biasing the anti-parallel diode from the complementary transistor. As the diode starts conducting and all the transistors are turned off, the voltage at the converter output becomes defined by the current direction and changes its polarity. The rectifier voltage on the other hand stays the same for the same reason. Assuming the current direction is positive, this means that the voltage drop across the resonant tank suddenly changes from $V_{in} - V_{out}$ to $-V_{in} - V_{out}$. This quickly brings the inductor current down to zero where it remains during the remainder of the switching period as all the rectifier diodes become reverse-biased. At the beginning of the next switching period, the complementary transistor gets turned on and the inductor current starts from zero again.

4.3 Discontinuous conduction mode

According to [2], the condition for discontinuous operation is given by

$$\frac{f_s}{f_{res}} < \frac{V_{out}}{V_{in}} \tag{28}$$

This means that the converter enters the discontinuous conduction mode when the ratio of the switching and resonant frequency is lower than the inverse DC voltage ratio. Moreover, the DC voltage ratio rounded down to the nearest integer corresponds to the number of complete conduction half-cycles of the inductor current within one half of the switching period. Therefore it is useful to define the discontinuous conduction mode index as

$$k_d = \lfloor k_v \rfloor \tag{29}$$

The current and voltage waveforms are shown for k_d factor of 2. The circuit parameters remained the same as in the previous section for easier comparison.

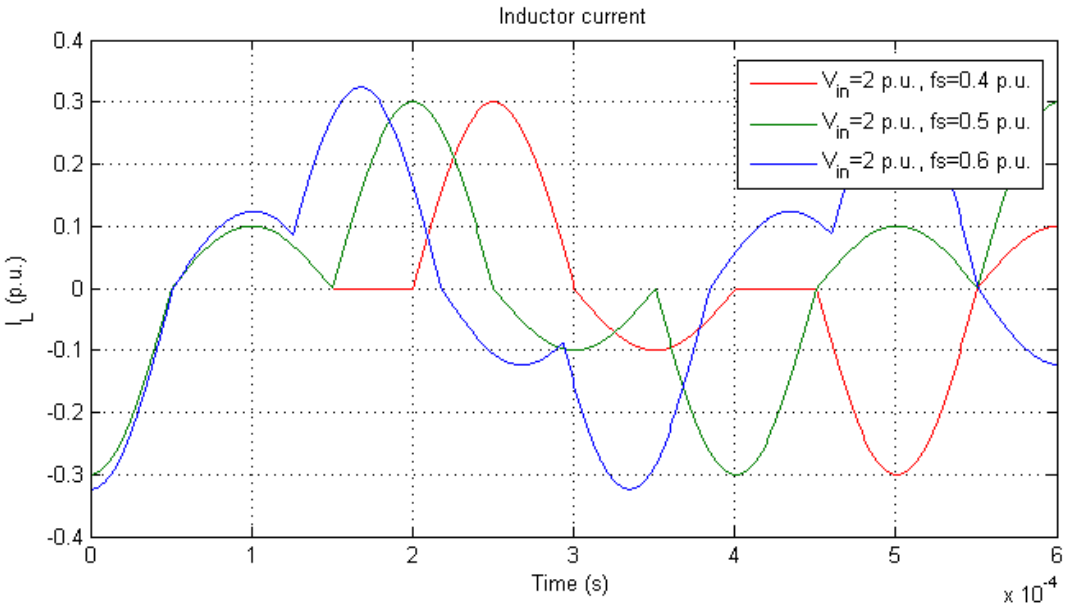

Figure 19 - Inductor current waveform in the discontinuous conduction mode

Figure 19 shows the inductor current waveform for 3 cases – with the frequency below, above and equal to 0.5 p.u. The waveforms are synchronized at the beginning of the diode conduction period. The red waveform shows the current during discontinuous conduction mode. The sequence starts with a soft IGBT turn-on due to the fact the inductor current is

zero. As the current grows, it charges the capacitor at the same time. Once the sum of the capacitor and the transformer's primary voltage exceeds the input voltage, the current reaches its maximum value and starts to drop back down to zero. At the zero-crossing instant the current reverses, the IGBT turns off softly and the antiparallel diode starts conducting. The capacitor discharges due to negative inductor current and continues to do so until the current reaches zero again. At this point, due to the amount of charge stored in the capacitor, the voltage on the secondary side of the transformer is lower than the load voltage. The rectifier bridge is reverse-polarized and therefore the inductor current remains zero until the end of the first half of the switching period, when the polarity of the converter output voltage changes and the next cycle, complementary to the previous one, starts.

For the switching frequency value of 0.5 p.u., the next conduction period starts right at the instance the previous one ends, making it a boundary between the continuous and discontinuous conduction mode. For the value of 0.6 p.u., the current does not stay at zero at any point, meaning the converter operates in the continuous conduction mode.

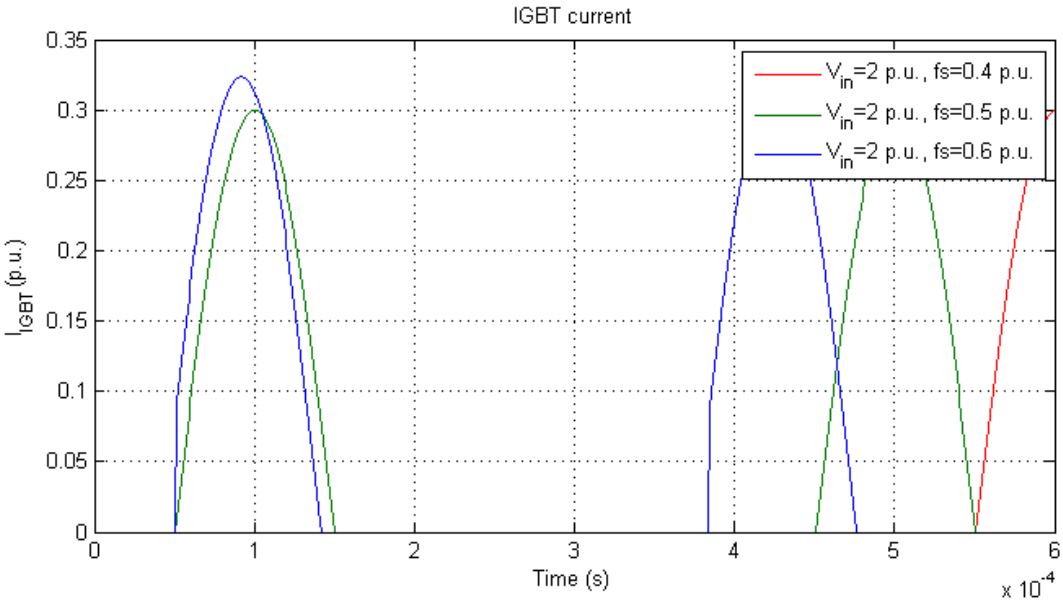

Figure 20 - IGBT current waveforms in the discontinuous conduction mode

The first big advantage of DCM over CCM is the reduction of switching losses due to soft turn-off and turn-on of switching devices. This is more closely shown in Figure 20. It is interesting to observe that the IGBT current waveform during one transistor conduction period

is identical for both the 0.4 and 0.5 p.u. frequency. This is also valid for the diode conduction period. This means that the discontinuous conduction mode is actually an array of the circuit's natural step responses. This is even more supported by the fact the inductor current rings with the resonant frequency during the conduction period.

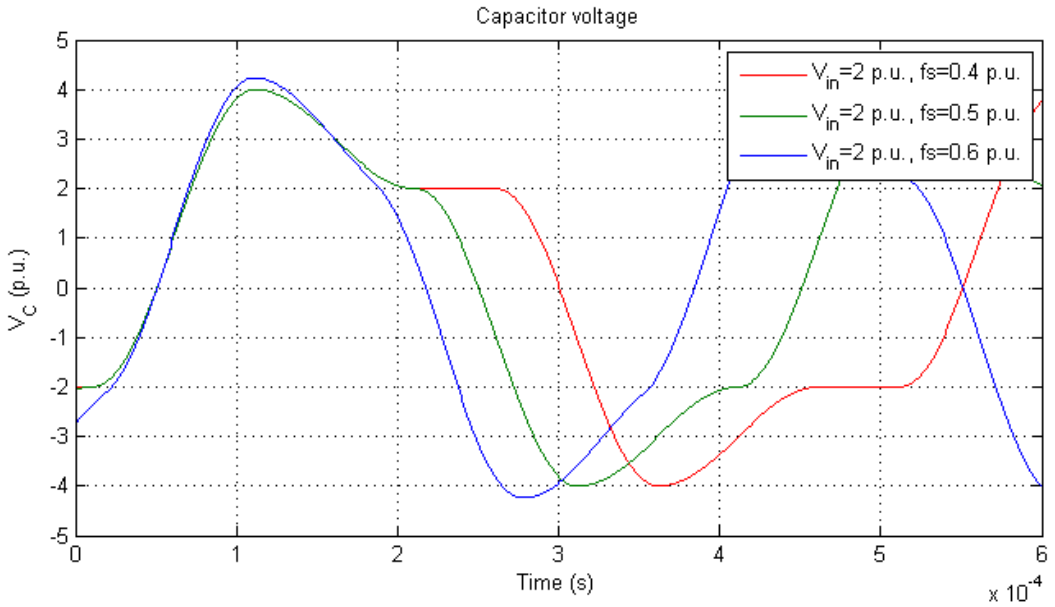

Figure 21 - Capacitor voltage waveform in the discontinuous conduction mode

The capacitor voltage waveform is shown in Figure 21. During the period when the inductor current is zero, the capacitor's charge does not change, meaning its voltage stays the same. This is visible on the red curve for the voltage values of ± 2 p.u. Similar to the inductor current, the capacitor voltage response is the same for switching frequency values below 0.5 p.u. The peak capacitor voltage is defined by the input voltage [3] as

$$\hat{v}_C = 2\,V_{in} \tag{30}$$

Equation (30) describes the second big advantage of the discontinuous conduction mode. The capacitor peak voltage stress is limited to only twice the value of the input voltage while in the continuous conduction mode, as shown before, the voltage stress can rise up to several dozens of times the input voltage. It should be however noted that (30) is valid only for type 2 DCM.

The biggest downside of this mode is the power transfer capability of the circuit. For the same component choice, the RMS value of the inductor current is significantly lower than in the continuous conduction mode. This means that a lot higher voltage difference is required to push the same amount of power through the circuit than in the continuous conduction mode. In other words, the discontinuous conduction mode trades off the MF transformer requirements in favor of the reduced capacitor voltage stress and lower switching losses.

Another disadvantage of the discontinuous conduction mode is the peak-to-RMS ratio of the inductor current. As already shown in Figure 19, the RMS current value can only be regulated by changing the amount of time the current through the inductor stays zero. Moreover, RMS value of the inductor current over one diode conduction cycle is lower than for an IGBT. Therefore, the lower the power reference, the higher will the peak-to-RMS ratio be. This means that the peak inductor current value will be a lot higher in DCM than CCM for the same amount of power transferred.

The peak-to-average ratio of the output current, and thus the peak-to-RMS ratio of the inductor current as well, can be improved by increasing the number of half-cycles in one switching period. Figure 22 shows the output current waveforms for type 2 and type 4 discontinuous conduction modes.

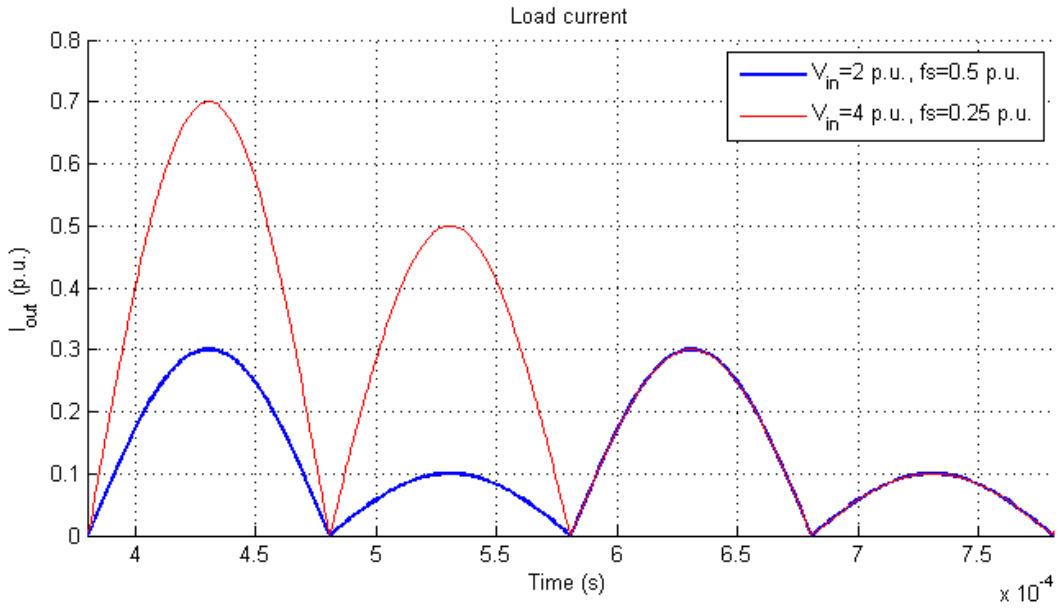

Figure 22 - Output current waveforms for type 2 and type 4 discontinuous conduction modes

When operating in the discontinuous mode at higher k_d factors, the resonant tank rings with a higher number of half-cycles within one half of the switching period. As visible from Figure 22, the ratio of two adjacent current peaks increases with the number of finished half-cycles. In other words, at the beginning of each half of the switching period, the difference between the peak current values of the first and second half-cycles is smaller than between the second and third and so on. This property can be written as

$$\frac{\hat{I}_{out}(n)}{\hat{I}_{out}(n+1)} < \frac{\hat{I}_{out}(n+1)}{\hat{I}_{out}(n+2)}\Bigg|_{n=1,2,3\dots k_d-2} \tag{31}$$

where n is index of the half-cycle. During each of the half-cycles, the output current is a sine wave of the resonant frequency with a fixed amplitude. The average current value over one half of the switching period can be calculated using

$$I_{out} = \frac{2}{T_s}\int_0^{\frac{T_s}{2}} i_{out}(t)dt \tag{32}$$

During that time, the output current rings with k_d number of half-cycles which all have the same duration. Expanding (32) gives

$$I_{out} = \frac{2}{k_d T_{res}}\sum_{n=1}^{k_d}\int_0^{\frac{T_{res}}{2}} \hat{I}_{out}(n)\ \sin(\frac{2\pi}{T_{res}}t)\,dt \tag{33}$$

Finally, solving (33) yields

$$I_{out} = \frac{2}{\pi k_d}\sum_{n=1}^{k_d}\hat{I}_{out}(n) \tag{34}$$

Equation (34) gives a simple way of calculating the average value of the output current if the peaks of each half-cycle are known. The peak of the whole waveform over one half of the switching period is the peak of the first half-cycle. The average-to-peak ratio can therefore be expressed as

$$\frac{I_{out}}{\hat{I}_{out}} = \frac{2}{\pi k_d} \sum_{n=1}^{k_d} \frac{\hat{I}_{out}(n)}{\hat{I}_{out}(1)} \tag{35}$$

Using the properties obtained in (31) and (35), it can be shown that

$$\frac{I_{out}}{\hat{I}_{out}}(k_{d1}) > \frac{I_{out}}{\hat{I}_{out}}(k_{d2}) \,\Big|\, k_{d1} > k_{d2} \tag{36}$$

This means that an increase in k_d factor improves the average-to-peak ratio of the output current.

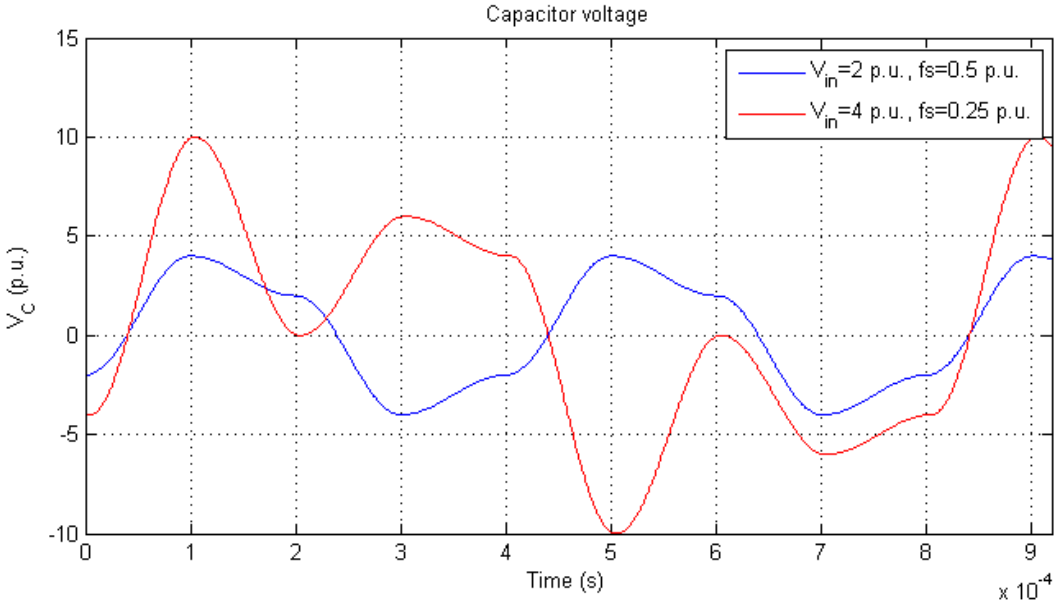

Figure 23 - Capacitor voltage waveforms for type 2 and type 4 discontinuous conduction modes

Figure 23 shows the capacitor voltage waveforms for the same case. For the type 4 conduction mode, the peak capacitor voltage rises to 2.5 times the value of the input voltage. However, since the input voltage had already been increased 4 times its nominal value, this results in 10 p.u. capacitor peak voltage. This is comparable to the voltage stresses in the continuous conduction mode as shown in Figure 12, but with a much worse peak-to-RMS ratio and lower average output current. The approach of increasing the input voltage to enter the discontinuous conduction mode is therefore not feasible.

However, for this particular application, the input and output voltages levels will both be fixed. This means that the only possibility to alter the voltage transfer ratio is by changing the transfer ratio of the MF transformer within the converter. Increasing the number of turns on the secondary side effectively lowers its voltage as perceived by the primary side. Therefore, the effective DC voltage transfer ratio is given by

$$k_v' = \frac{N_2}{N_1} \cdot \frac{V_{in}}{V_{out}} \tag{37}$$

where N_1 is the number of turns on the primary and N_2 the number of turns on the secondary side of the MF transformer. The output current waveforms for the same conduction type modes are shown in Figure 24. The currents have been recalculated to the primary side.

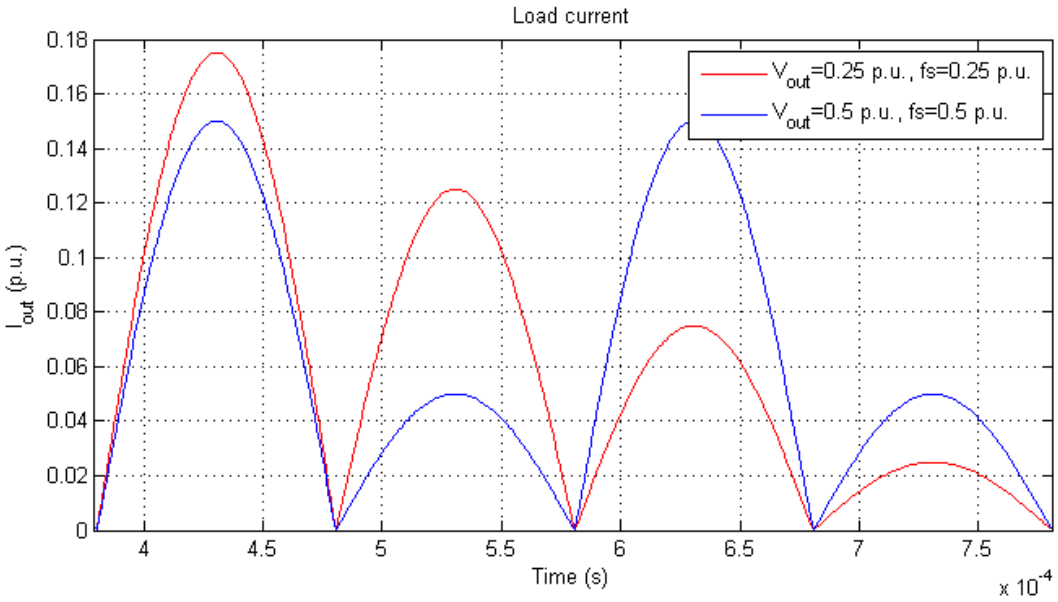

Figure 24 - Output current waveforms for discontinuous conduction modes with the lower MVDC side

In comparison with Figure 22, the current waveforms stay practically the same, but with much lower peak values. Moreover, the current gain achieved by increasing the k_d factor from 2 to 4 is significantly lower. This is a natural consequence of having a lower voltage difference between the input and the output compared to when the input voltage was increased.

The capacitor voltage waveforms are shown in Figure 25. The capacitor peak-to-input voltage ratio stayed the same as before, 2 for type 2 and 2.5 for type 4 conduction modes.

However, since the input voltage is now lower, so is the peak voltage stress. Otherwise the waveforms stayed the same, simply scaled by a constant.

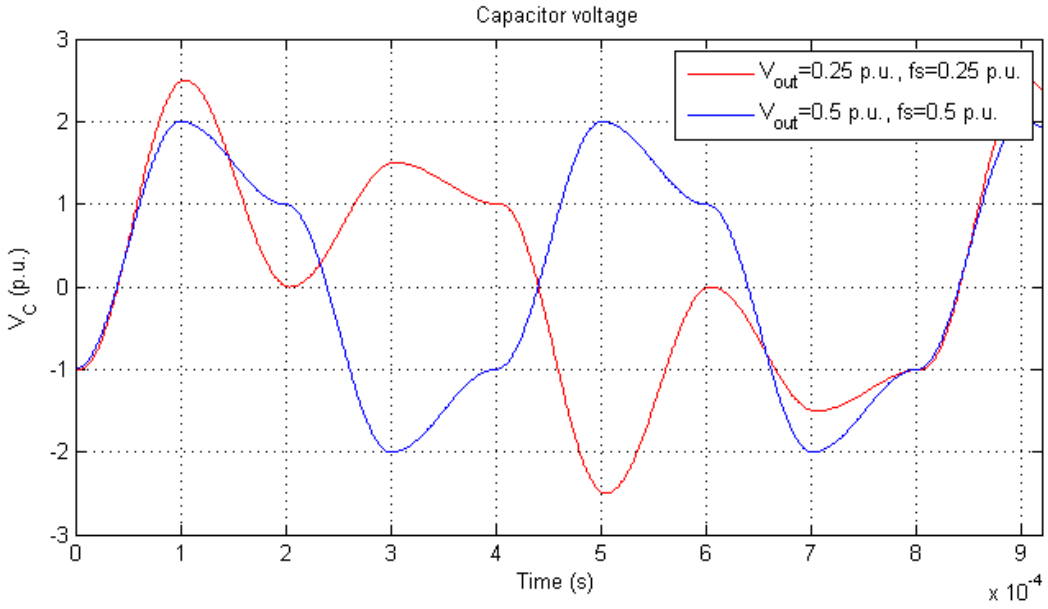

Figure 25 – Capacitor voltage waveforms for discontinuous conduction modes with the lower MVDC side

Overall, due to the fact the increase in current does not proportionally follow the decrease in voltage, the output power decreases with the k_d factor when only the transformer transfer ratio is altered. This is shown in Figure 26. Since k_d is an integer, the curve had been fitted with a 5th order polynomial for easier readability.

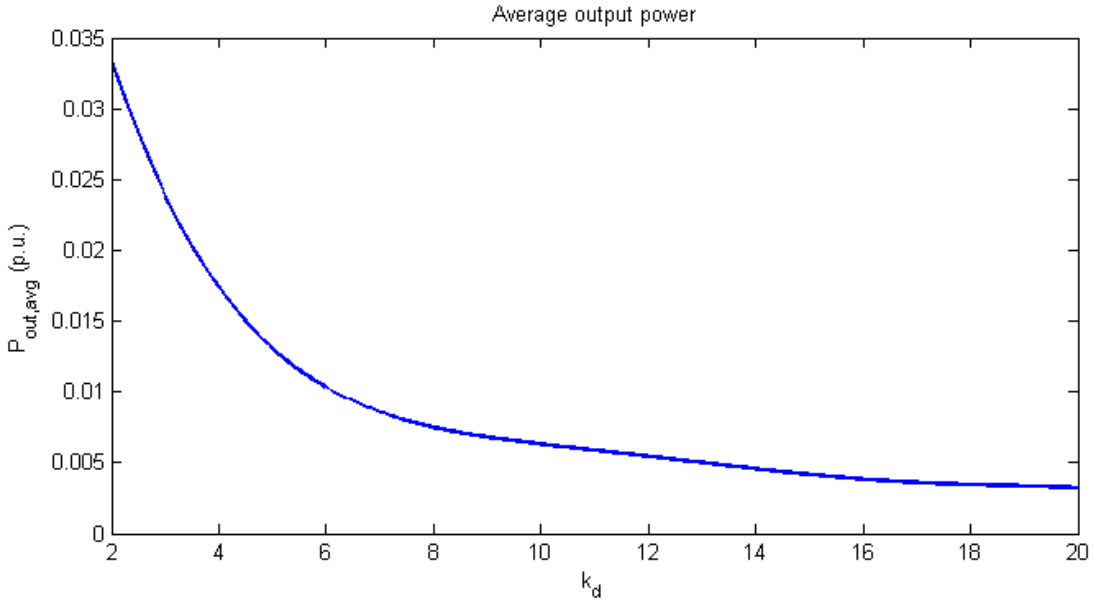

Figure 26 - Average output power dependence on discontinuous conduction mode type

The figure shows that, for this and similar high power transfer applications, it is almost obligatory to use k_d factor of 2. Moreover, looking at the output power values, it is visible that they are far below the desired level. This means that a resonant tank with a much higher characteristic admittance value has to be selected for operation in DCM compared to CCM.

Since the analysis was performed at the boundary condition of the DCM, with the inductor current not staying at zero, Figure 26 also depicts the maximum power transfer that can be achieved in each of the modes. Therefore, if the converter needs to operate solely in DCM, the L and C component selection has to be made in such a way that the maximum power transfer is achieved when it operates on the boundary between the two conduction modes.

4.4 Power relations

In this particular application, the resonant converter will be used to control the output power. In order to design a controller, relations between the output power and the switching frequency need to be obtained. The known variables are the input and output voltages, transformer turns ratio and resonant tank's inductance and capacitance values. The circuit is still assumed to be ideal.

As stated before, in the continuous conduction mode, the capacitor and the inductor waveforms can be approximated by ideal sinusoidals. Starting from the result obtained in (25) and including the transformer turns ratio, the average output power can be written as

$$P_{out} = \frac{2\sqrt{2}}{\pi}\frac{N_1}{N_2}V_{out} \cdot \sqrt{V_{in}^2 - \left(\frac{N_1}{N_2}V_{out}\right)^2} \cdot \left|\frac{2\pi f_s C}{1 - 4\pi^2 f_s^2 LC}\right| \tag{38}$$

The equation can be simplified by recalculating the output voltage to the transformer's primary side as

$$V'_{out} = \frac{N_1}{N_2}V_{out} \tag{39}$$

Then, solving (38) for f_s gives

$$f_s = \left| V'_{out}\frac{C\sqrt{V_{in}^2 - V'^2_{out}} \pm \sqrt{C^2(V_{in}^2 - V'^2_{out}) + \sqrt{2}\pi LC\left(\frac{P_{out}}{V'_{out}}\right)^2}}{\sqrt{2}\pi^2 LCP_{out}} \right| \tag{40}$$

Equation (40) gives an explicit relationship between the desired power output and the switching frequency when the converter operates near the resonance region and can be used for feed-forward control of the converter. If the sign is negative, the converter will operate in the sub-resonance region, while for the positive, in the super-resonance region.

Equation (38) also gives information about the optimal transformer transfer ratio for maximizing the power transfer. For a constant switching frequency, the expression can be rewritten as

$$P_{out} = K \cdot V'_{out} \cdot \sqrt{V_{in}^2 - V'^2_{out}} \tag{41}$$

where K is a generic constant. Normalizing K as 1 and V_{in} as 1 p.u. , the values of P_{out} from (41) over the practical range of V'_{out} have been plotted in Figure 27.

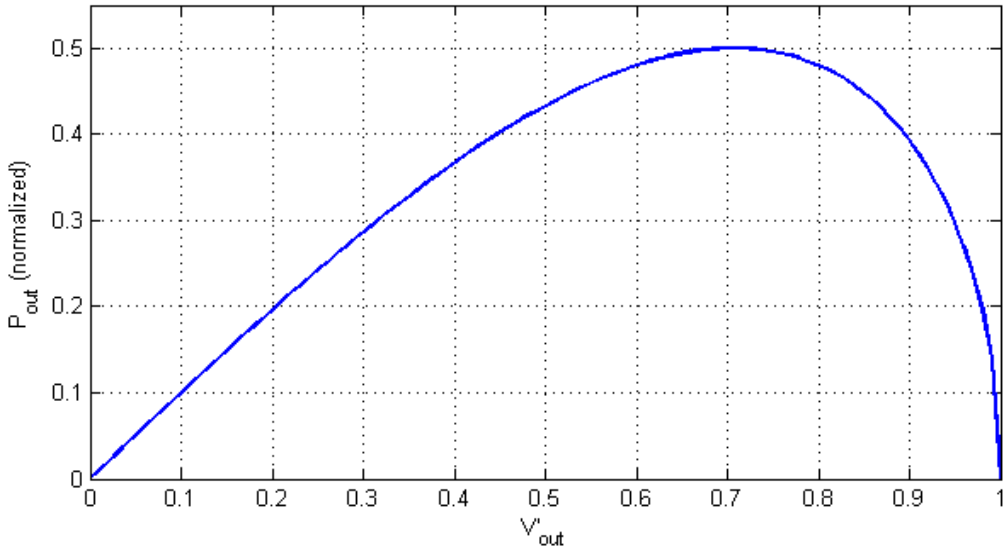

Figure 27 - Normalized output power dependence on output voltage at fixed switching frequency

The criteria for obtaining the maximum output power can be obtained by derivating the expression and finding a stationary point. Solving the problem for V'_{out} yields one feasible solution:

$$V'_{out} = \frac{V_{in}}{\sqrt{2}} \tag{42}$$

This means that the maximum power transfer is reached when the output voltage as perceived by the primary side is $\sqrt{2}/2$ times lower than the input voltage. The numerical value of (42) for the case shown in Figure 27 is ≈ 0.707, which coincides with the graph. Therefore, the optimal transformer transfer ratio can be calculated as

$$\frac{N_1}{N_2} = \frac{V_{in}}{\sqrt{2}\, V_{out}} \tag{43}$$

For the discontinuous conduction mode, the resonant tank does not have a sinusoidal response anymore and therefore (40) cannot be applied. The power equation can be derived from the responses shown in Figure 28. This is done for the k_d factor of 2.

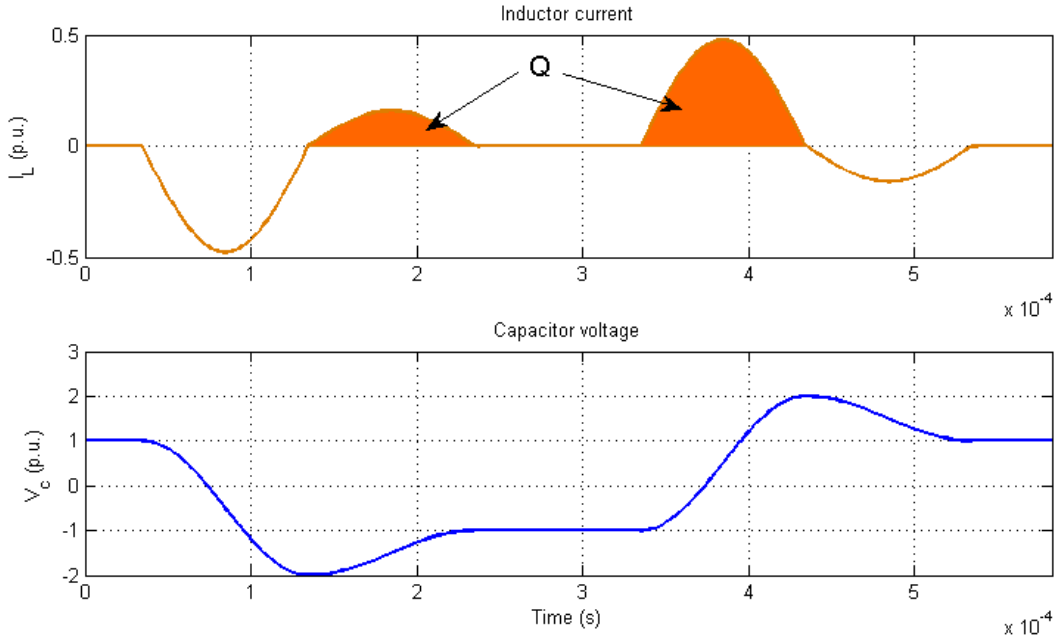

Figure 28 - Inductor current and capacitor voltage responses for deriving the power equation

From the moment the antiparallel diode start conducting until the transistor turns off naturally, a positive charge, represented by the area under the orange curve, flows into the capacitor. During that period, the capacitor voltage changes from $-2V_{in}$ to $+2V_{in}$. Knowing the capacitance value, the area under the curve can be calculated as

$$Q = 4 \cdot C \cdot V_{in} \tag{44}$$

During the same period, the average inductor current is equal to

$$\langle i_L(t) \rangle_{T_s} = 2 \cdot Q \cdot f_s \tag{45}$$

The same current, scaled by the transformer's transfer ratio, flows through the passive rectifier on the secondary side of the transformer. The passive rectifier supplies the load with

the current of the same magnitude and a positive sign. This means that the scaled average output current is the same as the average inductor current given by (45). If the transformer is ideal, the power on its primary side is the same as the power on its secondary. Therefore, an expression linking the average output power to the switching frequency can be obtained by combining (39), (44) and (45) as

$$P_{out} = 8 \cdot C \cdot V_{in} \cdot V'_{out} \cdot f_s \tag{46}$$

Comparing (40) and (46), it is clear that controlling the power is much simpler in the discontinuous conduction mode. The latter expression also indicates that the output power is proportional to the output voltage, which, under the limitation of (28), means that the maximum power transfer is achieved when

$$\frac{N_1}{N_2} = \frac{V_{in}}{2\,V_{out}} \tag{47}$$

Moreover, since the switching frequency is limited, the maximum power transfer that can be achieved in the discontinuous conduction mode can be calculated using (4), (46) and (47), which yields

$$P_{out,max} = \frac{V_{in}^2}{\pi}\sqrt{\frac{C}{L}} \tag{48}$$

This means that the output power is proportional to the characteristic admittance of the resonant tank. Equation (48) is very useful for dimensioning the resonant tank components when the output power requirement is known.

4.5 Loss estimation

Since the converter will be used for high power applications, it is important to be able to accurately estimate its losses. The calculated losses can afterwards be used for estimating the working temperature of the converter and dimensioning the cooling system. They can also be used for evaluating the overall conversion efficiency and thus assessing the financial feasibility of such a solution. The total power loss will be distributed over the 4 main components – the IGBT bridge, the resonant tank, the MF transformer and the passive rectifier.

The total IGBT bridge loss can be calculated as a combination of transistor losses and diode losses. These can furthermore be divided into two categories – the conduction losses and the switching losses. For the conduction losses calculation, the IGBT can be approximated by a series connection of a resistor, representing the on-state collector-emitter resistance, and a voltage source, representing the on-state zero-current collector-emitter voltage [4]. The analogous approximation can be applied to the anti-parallel diode, giving

$$u_{CE} = u_{CE0} + r_{CE} i_C \tag{49}$$

$$u_D = u_{D0} + r_D i_D \tag{50}$$

The instantaneous power loss can therefore be calculated as a product of voltage and current. The average conduction losses over one switching period can be calculated as

$$P_{CT} = \frac{1}{T_s} \int_0^{T_s} [u_{CE0} i_C(t) + r_{CE} i_C^2(t)]\, dt \tag{51}$$

$$P_{CD} = \frac{1}{T_s} \int_0^{T_s} [u_{D0} i_D(t) + r_D i_D^2(t)]\, dt \tag{52}$$

Solving (51) and (52) gives

$$P_{CT} = u_{CE0}\, I_{C,avg} + r_{CE}\, I_{C,rms}^2 \tag{53}$$

$$P_{CD} = u_{D0}\, I_{D,avg} + r_D\, I_{D,rms}^2 \tag{54}$$

Conduction losses in the off-state on the other hand can be neglected due to very low leakage current values.

The switching losses are typically very demanding to calculate analytically [5], [6] and require numerous parameters of which some often cannot be found in the manufacturer's datasheets. Another approach is to use computer simulation tools to calculate the switching losses. However, since the switching transients occur at the level of nanoseconds, a very small time step is required to solve such systems and the models still require a great number of parameters.

The simulation tool used is Plecs, which simulates electrical circuits on a system level. To solve them at high speed, all the switching devices are modelled as ideal switches, meaning that the current and voltage changes are instantaneous. The switching losses will therefore be estimated by capturing the current and voltage values at the switching instances and using the lookup tables provided by device manufacturers to determine the energy loss at each instant.

The same methods as the ones described above can be used to calculate the rectifier losses.

The resonant tank will generate losses due to series resistance of an inductor and a capacitor. The average power loss can be calculated as

$$P_{tank} = (R_L + R_C)\, I_{L,rms}^2 \tag{55}$$

The transformer losses can be divided into two categories – core losses and copper losses. Core losses consist of hysteresis and eddy current losses. These losses can be very accurately estimated in the conventional transformers excited by 50/60 Hz sine waves. However, since the MF transformers are normally excited by rectangular waveforms and at much higher frequencies, the loss estimation gets a lot more complicated [7], [8].

The hysteresis losses are proportional to the frequency, while the eddy current losses to the frequency squared. The fact that resonant converters operate by altering the switching frequency makes the analysis even more complicated. The equivalent electrical scheme of the transformer would need to use variable inductances and resistances to compensate for the change in the excitation frequency.

The MF transformers have a much higher ratio of core losses in the overall losses due to significantly higher frequencies they operate in. However, thanks to the new materials used in MF transformer's core and windings, their overall losses are comparable to the ones of conventional transformers [9], with efficiencies exceeding 99%. Therefore, the transformer core losses will be neglected. Since the resonant tank's inductor is often integrated in the transformer, the conduction losses of the resonant tank will include the transformer conduction losses in this simulation.

Most important points stated in this chapter are the following:

- Series-resonant converter circuit can be modelled using 3 linear circuits if the switching frequency is close to the resonant frequency
- Input voltage always has to be higher than the output voltage scaled by the transformer's transfer ratio, otherwise no power can be transferred
- Component stress increases significantly as the switching frequency approaches the resonant frequency
- Capacitor voltage is independent of the choice of L and C values, which makes it possible to design a resonant tank based on the maximum permissible capacitor voltage and output power requirements
- As a general rule, the lower the inductance and higher the capacitance, the greater the amount of power that can be transferred through the circuit
- Addition of dead time to the control signal does not influence the circuit's performance as long as the duty cycle remains above 85%
- Two biggest advantages of DCM compared to CCM are zero current switching and limited capacitor voltage
- Increasing the number of conduction half-cycles in DCM improves the peak-to-average ratio of the output current, but increases the peak capacitor voltage and reduces the amount of power that can be transferred through the circuit
- A lot higher characteristic admittance of resonant tank components is required to transfer the same amount of power in DCM compared to CCM
- The choice of transformer's transfer ratio influences the amount of power that can be transferred through the circuit and its optimal value is different for CCM and DCM
- Relationship between the output power and switching frequency is linear in DCM while highly nonlinear in CCM. This means that DCM converters require a substantially simpler control system

5 Resonant converter design

5.1 Component selection

This section proposes a 10 MW circuit configuration. The necessary input parameters are voltage levels and output power. Wind turbine generators are normally rated at 690 V. However, since the subject of this analysis is a 10 MW wind turbine, an assumption will be made that a 3.3 kV generator is used to reduce the current rating of the components. Another assumption is that the turbine uses a passive rectifier with a large DC link capacitor at its output. This means that the converter input voltage will be equal to the peak value the rated generator voltage, giving

$$V_{LVDC} = \sqrt{2} \cdot 3300\ V \approx 4667\ V \tag{56}$$

At the same time, the MVDC voltage level will be rated at 35 kV. The chosen switching frequency is 5000 kHz.

Based on previous observations, a DC-DC resonant converter circuit can be designed. Due to reduced switching losses and lower component voltage stress, discontinuous conduction mode has been chosen for the whole operating range. In accordance with the conclusions made in the previous section, k_d factor of 2 has been selected. Assuming the input and output voltages will not change more than ± 10% in normal operation, the transformer transfer ratio can be calculated using (47) as

$$\frac{N_2}{N_1} = \frac{2 \cdot 1.1 \cdot V_{MVDC}}{0.9 \cdot V_{LVDC}} \approx 19 \tag{57}$$

The transfer ratio calculated in (57) has been rounded up to the nearest integer to ensure the converter stays in type 2 DCM. Having the transformer transfer ratio selected, the required resonance tank's capacitance can be calculated using (46). Since the converter should be able to operate in DCM at all times, this gives

$$C = \frac{P_{out}}{4 \cdot f_{res} \cdot 0.9^2 \cdot V_{LVDC} \cdot V'_{MVDC}} = 71.8\ \mu F \tag{58}$$

The inductance value can be obtained from (4) as

$$L = \frac{1}{4\pi^2 f_{res}^2\, C} = 14.1\ \mu H \tag{59}$$

The resonant tank components need to be designed to withstand the peak voltage and current stresses. The peak capacitor voltage stress is given by (30), which yields

$$\hat{v}_C = 2 \cdot V_{LVDC} = 9334\ V \tag{60}$$

The peak current stress is difficult to calculate and therefore has been obtained by simulation, which yielded 14.8 kA. The result indicates that it would be beneficial to split the converter circuit into several identical parallel modules. The benefits of doing so are reduced component current ratings, reduced conduction losses and increased redundancy. On the other hand, this will make the control system more complex.

Splitting resonant converters into modules cannot be done by simply taking several previously designed modules and connecting them in parallel. The reason for that is given by Figure 28. The basic principle of controlling the average output power in DCM is by changing the switching frequency and therefore creating a longer time period over which the power will be averaged. This is also given by equation (46). However, the peak current value will remain the same as it depends on the amount of charge stored in the capacitor, which is in return proportional to the input voltage. Therefore, connecting the modules in parallel would not reduce their peak current value, but simply the time between two peak instances.

To split the resonant converter into several modules, their capacitance and inductance values need to be scaled. If the converter should to be split into n_m modules, the capacitance and inductance values of each module can be calculated from the earlier obtained values as

$$C_{mod} = \frac{C}{n_m} \tag{61}$$

$$L_{mod} = L \cdot n_m \tag{62}$$

This solution will propose splitting a converter into 4 modules, which means that each module will have a power rating of 2.5 MW. The new capacitance and inductance values are therefore

$$C_{mod} = 17.95\ \mu F \tag{63}$$

$$L_{mod} = 56.4\ \mu H \tag{64}$$

Using these values, peak current was brought down to 3.7 kA, which coincides with the expected results. The frequency characteristic of the converter did not change, meaning that the nominal operating point remained the same.

Finally, it is useful to know the peak energy stored in the components for their dimensioning. The peak capacitor and inductor energy per module can be calculated using

$$E_{C,mod} = C_{mod} \cdot \frac{\hat{v}_C^2}{2} = 782\ J \tag{65}$$

$$E_{L,mod} = L_{mod} \cdot \frac{\hat{\imath}_L^2}{2} = 386\ J \tag{66}$$

The results show that, since resonant converters operate at high frequencies, the peak energy stored in each of the resonant tank components is relatively low compared to the power rating of the circuit. This is one of the factors that can lead to a reduction in size and weight.

5.2 Control system

The proposed control system diagram is shown in Figure 29.

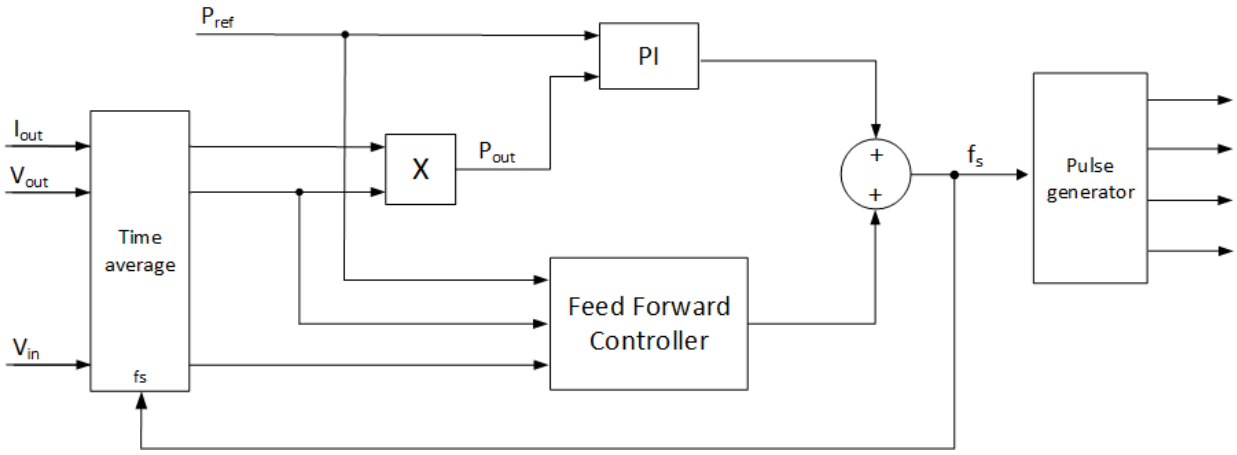

Figure 29 - Control system layout

The input parameters are the power reference, input and output voltage measurements and the output current measurement. These 3 quantities provide base inputs for the control system, which is implemented as a combination of a feed-forward and a feedback controller. All the measurements need to be averaged over one switching period, but since the switching frequency changes during operation, variable time sampling needs to be used. The switching frequency is therefore fed back to the time average block, which uses it to determine the length of the averaging period. The averaging period is updated only once the previous one is over, meaning that intermediate changes in the frequency reference imposed by the PI controller do not have an impact on its value. The same rule applies for the pulse generator. The pulse frequency is updated only once the previous switching period finishes, as updating the switching frequency continuously would create jitter, harmonics and DC offset in the converter output voltage, rendering the circuit unstable.

The feed-forward controller implements the control law given by (46). Since the equation was derived from an idealized circuit, the imperfections such as the switch on-resistance or the resonant tank's series resistance will cause some losses and therefore the actual power output will be lower than calculated. The purpose of the PI controller is to adjust the frequency reference to compensate for the difference between the idealized model and the real circuit.

It is possible that, due to some unpredictable events, such as voltage fluctuations exceeding the 10% tolerance level for example, the converter cannot temporarily deliver the desired amount of power while operating in the discontinuous conduction mode. The control will respond on two levels.

First, if the cause for such a behavior is due to a voltage drop in the input or an increase in the output voltage of an unexpected magnitude, the feed-forward controller will give out a new power reference which will be above the half of the resonant frequency. This will cause the circuit to enter the continuous conduction mode, thus making the power relation (46) invalid. However, as shown in Figure 19 and Figure 21, at these frequencies the current and voltage responses are still highly non-sinusoidal, meaning that the power relation for the continuous conduction mode given by (40) cannot be used either. At the same time, the current and voltage waveforms resemble the discontinuous conduction waveforms a lot closer than the ones of near-resonant operation, meaning that the difference between the calculated and the actual output power will be relatively small. This is shown in Figure 30 on the example of a proposed 2.5 MW module. The difference gets bigger as the frequency increases, but since the switching frequency should not drift far away from 2500 Hz, the error will stay small and be easily handled by the PI controller.

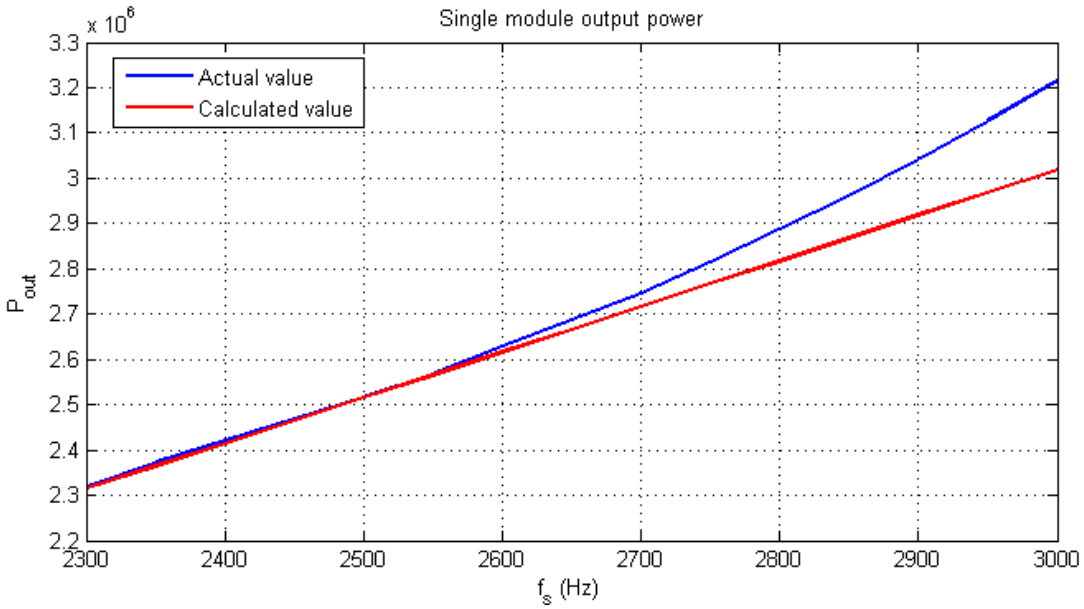

Figure 30 - Actual and calculated output power dependence on switching frequency

Second, regardless of the cause of the disturbance, the PI controller will register a difference between the actual power and its reference and increase the switching frequency. However, since entering the continuous conduction mode will also lead to increased voltage and current stress of the components, it is also important to monitor their values and implement protection mechanisms.

A two-level protection scheme with both soft and hard stop is proposed. Since circuit protection is only marginally covered by the scope of this project, an example will be given on inductor protection. The protection system schematic is shown in Figure 31.

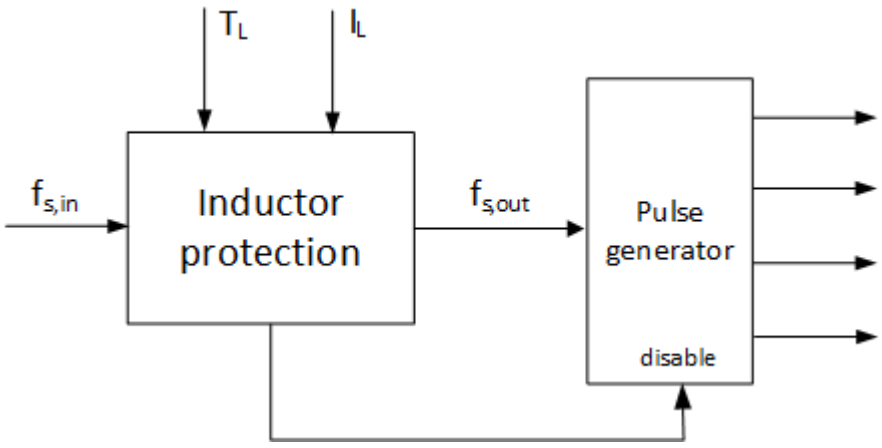

Figure 31 - Inductor protection mechanism

The protection system is connected between the frequency reference summation point and the pulse generator from Figure 29. The monitored quantities are the inductor current and temperature. The inductor might or might not be integrated in the transformer. During normal operation, the inductor protection block acts as a direct feed through for the frequency reference. In case the circuit goes into temporary and permissible overload, the soft stop mechanism adjusts the frequency reference to keep the inductor temperature within permissible limits. Since the inductor's thermal constant is a lot higher than the electrical, this means that the switching frequency will stay intact at first once it enters the soft stop zone, but as time passes, the increase in the inductor temperature will cause the protection system to decrease the switching frequency more and more, until either the temporary event passes

and the converter returns to normal operating state, or hard stop protection gets triggered. Hard stop protection monitors if the measured quantities are below their highest permissible values. In case the overload lasts for too long and the inductor temperature increases too much, or an abrupt load voltage drop causes the inductor current to grow very fast above its nominal value, hard stop protection will trip and switch the converter off instantaneously.

While the converter is in off state, no energy is stored in its components. This means that the capacitor voltage and inductor current are equal to zero. Once the converter gets turned on, it takes several cycles to reach the steady-state operating point. The transient response of the converter contains overshoots due to balancing of energy storage elements. As the controller response time between two consecutive reference adjustments is one switching period, these transients cannot be controlled as they appear at the resonant frequency. Current and voltage overshoots would most likely trip hard-stop protection mechanisms, turning the converter off before it even started up.

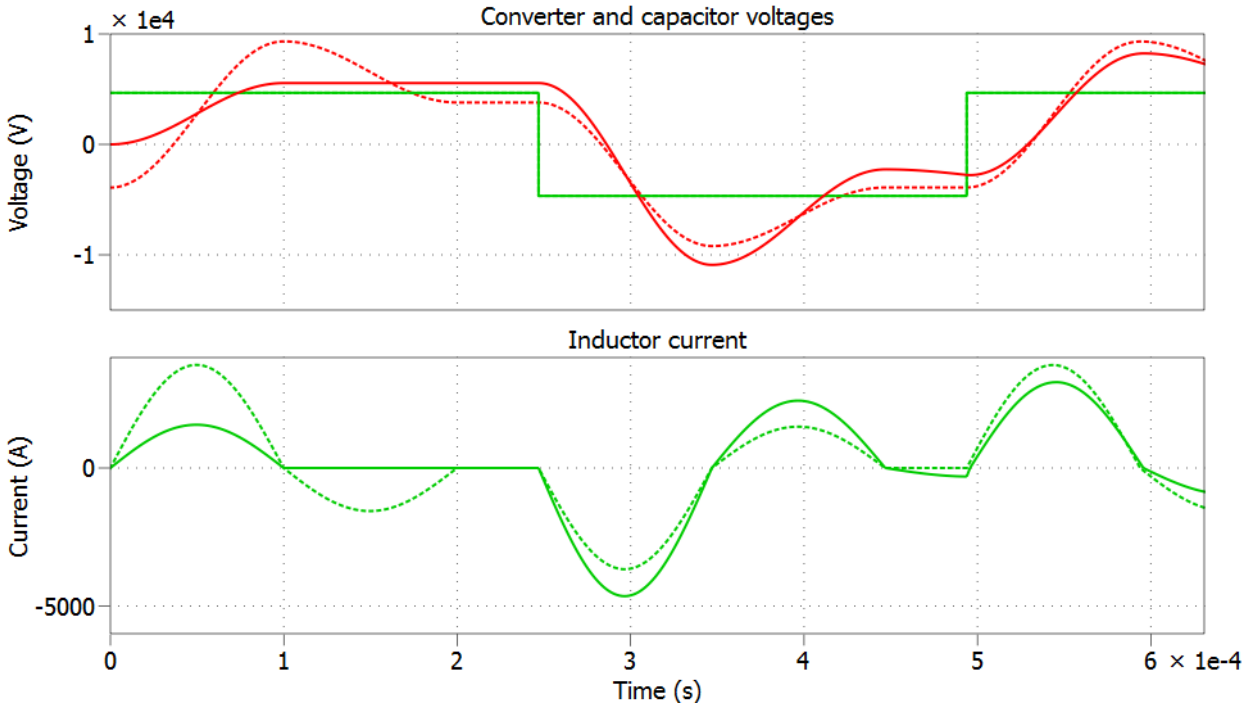

Figure 32 - Capacitor voltage and inductor current waveforms during startup (full line) and steady state (dotted)

This problem can, however, be solved using a capacitor pre-charge mechanism. As stated before, current and voltage overshoots occur due to a difference between the amount of energy stored in the capacitor and the inductor in steady-state and at the moment of

starting the converter up, when they are both assumed to be zero. Observing Figure 32, it is clear that, within one switching period, the inductor current crosses zero four times. Since the inductor current is also zero when the converter is off, pre-charging the capacitor to either one of these voltage values would create the same conditions as if the converter was already in steady state, thus completely eliminating the overshoot. Four possible solutions have been obtained by simulation.

$$v_{C0-1,2} = \pm 9320\ V \tag{67}$$

$$v_{C0-3,4} = \pm 3675\ V \tag{68}$$

The amplitude of the first two solutions corresponds to approximately twice the input voltage, which had already been discussed in section 4.3. The small difference is caused by an added 1 mΩ resistor in order for the simulation to converge. The second solution pair is however more interesting, as the voltage amplitude is lower than the input voltage. Assuming the capacitor will be charged from the input source and not an external power supply, charging the capacitor to twice the input voltage would require an extra DC/DC converter to boost the voltage up. On the other hand, charging the capacitor to a lower voltage level than the input can be done with the addition of a simple resistor to limit the charging current. The proposed capacitor pre-charge solution is shown in Figure 33.

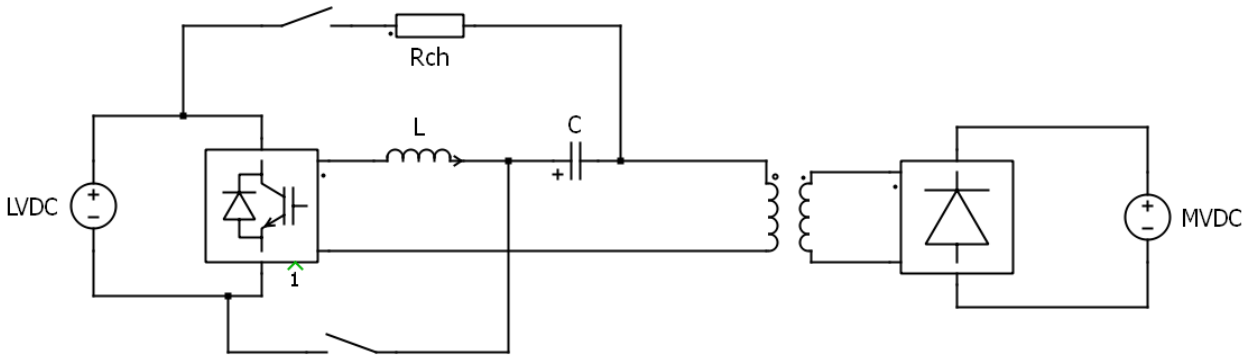

Figure 33 - Resonant converter circuit with a capacitor pre-charge mechanism

In case it is desired that the inductor current starts positive at the beginning of the first switching period, the capacitor should be pre-charged to -3675 V. The charging starts by

closing the switch, at which point a simple series RC circuit is formed. The capacitor voltage in this situation can be described by a well-known formula as

$$v_C(t) = -V_{LVDC}(1 - e^{-\frac{t}{R_{ch}C}}) \tag{69}$$

Increasing the charge resistor's magnitude increases the time constant of the circuit, which is in this case given by

$$\tau = R_{ch}C \tag{70}$$

The higher the time constant, the slower will the circuit respond and therefore the lower will the charging current be. By adjusting the resistance value, it is possible to determine at which time instant the capacitor voltage will reach (68) and thus when the charging circuit should disconnect. This can be calculated using

$$t_{C0} = -R_{ch}C \cdot \ln(\frac{v_{C0}}{V_{LVDC}} + 1) \tag{71}$$

The maximum charging current can be obtained from (69), which yields

$$i_{ch,max} = \frac{V_{LVDC}}{R_{ch}} \tag{72}$$

For the values of $C = 17.95\ \mu F$, $v_{C0} = -3675\ V$ and $R_{ch} = 100\ \Omega$, this results in

$$t_{C0} = 2.8\ ms \tag{73}$$

$$i_{ch,max} = 46.7\ A \tag{74}$$

The obtained time to charge is significantly higher than the controller response time, while the peak charge current is significantly lower than the peak current during normal operation. This means that the pre-charge mechanism does not introduce any additional requirements on the rest of the circuit and therefore provides a very cost-effective solution of eliminating the overshoot during startup operation.

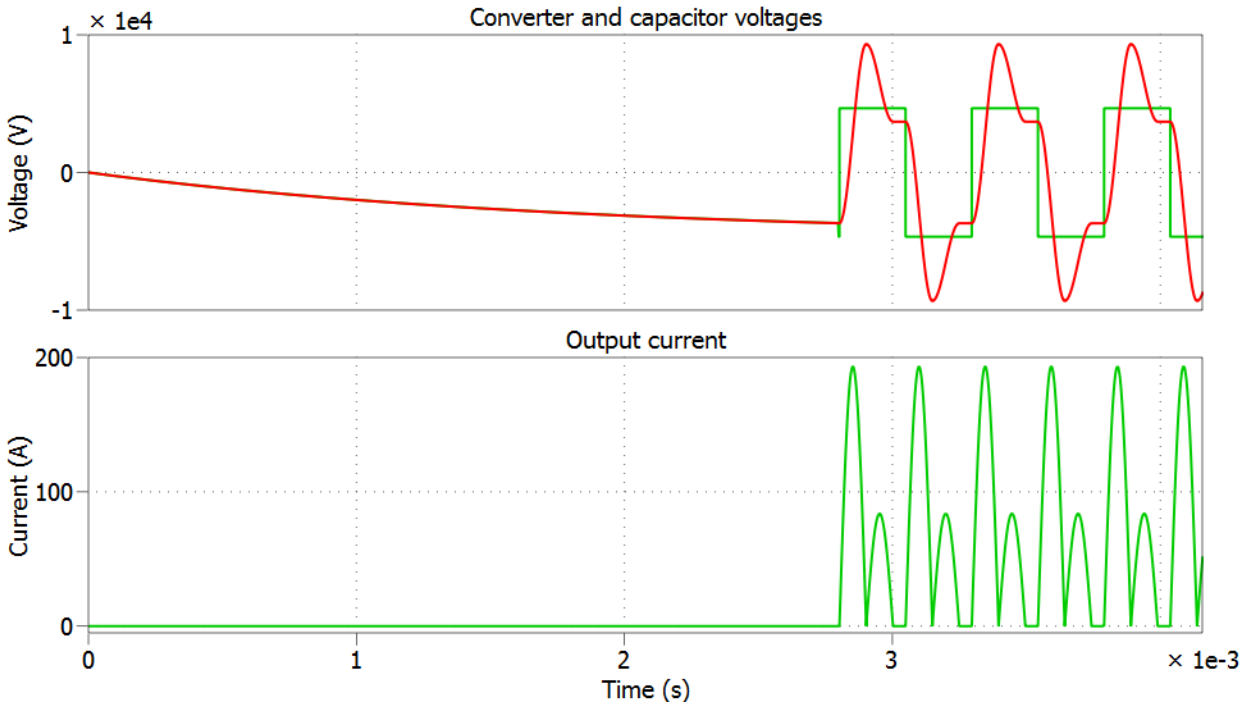

Figure 34 - Capacitor and input voltage and output current waveforms during a converter startup with a pre-charge mechanism

The converter startup sequence with the capacitor pre-charge circuit is shown in Figure 34. The converter starts operating at full power as soon as the charge circuit disconnects. As visible from the simulation results, the overshoot has been completely eliminated.

Most important points stated in this chapter are the following:

- Despite using a generator with significantly higher voltage rating than it is usual in conventional wind turbines, very high peak currents will likely require the converter to be split into several modules
- When splitting series-resonant converters into modules, resonant tank parameters need to be recalculated depending on the number of modules used. This does not change the converter's resonant frequency
- Since resonant converters operate at much higher frequencies than conventional converters, the amount of energy they store is significantly lower, which allows a reduction in their size and weight
- Feed-forward controller can be tuned using ideal circuit's parameters, while a feedback controller can be used to compensate for the difference between the ideal and real circuit
- The converter can temporarily operate in CCM in case the situation requires it, but the components should be monitored for overload
- Current and voltage overshoot during startup can be eliminated using a simple capacitor pre-charge circuit

6 Model validation

6.1 Laboratory setup

Laboratory setup schematic is shown in Figure 35. The main converter circuit consists of a 40 V voltage source, 68 µF DC link capacitors, full IGBT bridge, air-core inductor, resonant tank capacitor bank, MF transformer, full bridge rectifier and an active 40 V load. Auxiliary components include two gate driver circuits with their own multi-channel 0-30V/5V power supply, a signal generator and a scope with voltage and current probes.

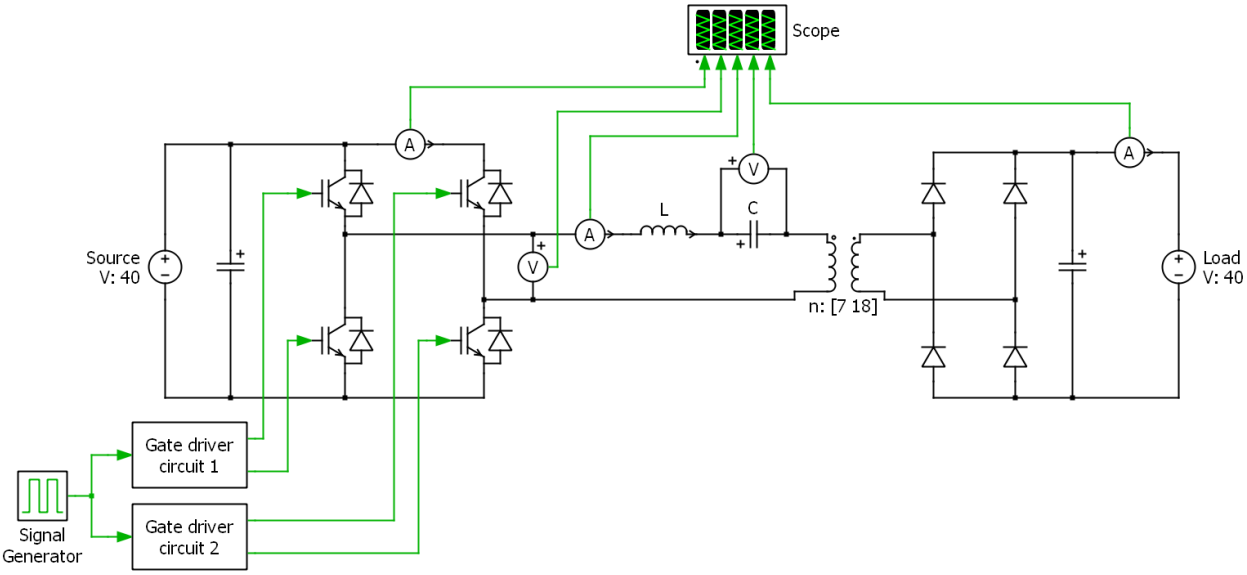

Figure 35 - Laboratory setup schematic

Nearly all of the setup components had to be built from parts. The medium frequency transformer, shown in Figure 36, was made using 4 E-shaped N87 silicon-ferrite half-cores, a coil former and wounded by hand using laminated copper wire. Primary and secondary windings were insulated using Mylar foil. Using the RLC meter, transformer's magnetization and leakage inductances, as well as winding resistances were obtained. The measurements were made at 10 kHz to ensure that skin effect and core nonlinearities occurring at higher frequencies are taken into account. Since the T/2 equivalent scheme was used for the simulation, the resistance and leakage inductance are given as lumped values transferred to the primary side. For practical reasons, the measured values for all the components are given in a single table at the end of this section.

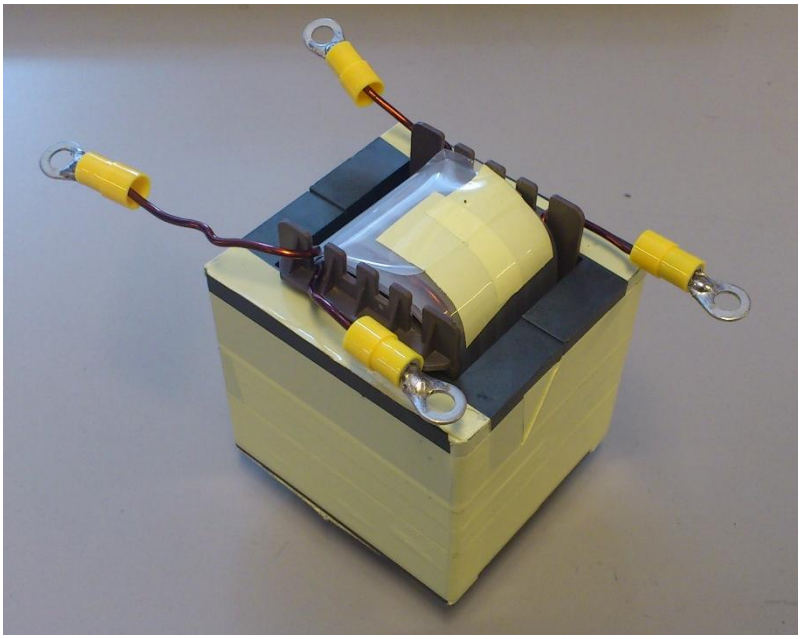

Figure 36 – Medium frequency transformer for the lab setup

Due to high current peaks that occur in DCM, it is important to ensure the transformer's core does not get saturated. Saturation flux density and core cross section can be extracted from the datasheet, while the peak magnetization current from simulation. Using these values it can be assessed whether the core will saturate or not. The core flux density was calculated using

$$B = \frac{L_m I_m}{N_1 A_{core}} = \frac{933\ \mu H\ \cdot 1.4\ A}{7 \cdot 1408\ mm^2} = 0.133\ T \tag{75}$$

From the material datasheet [10], the saturation flux density was obtained, being 0.4 T at 25 °C and 0.35 T at 100 °C. The calculated value from (75) is lower than both, meaning the transformer will not saturate even if it gets heated up.

Since the transformer's leakage inductance is lower than the required series inductance of the resonant circuit, an additional inductor had to be added to the circuit. Due to high peak currents the inductor will be exposed to, air core was selected to avoid problems with core saturation. The inductor is shown in Figure 37. It was formed using the same coil former model as the transformer.

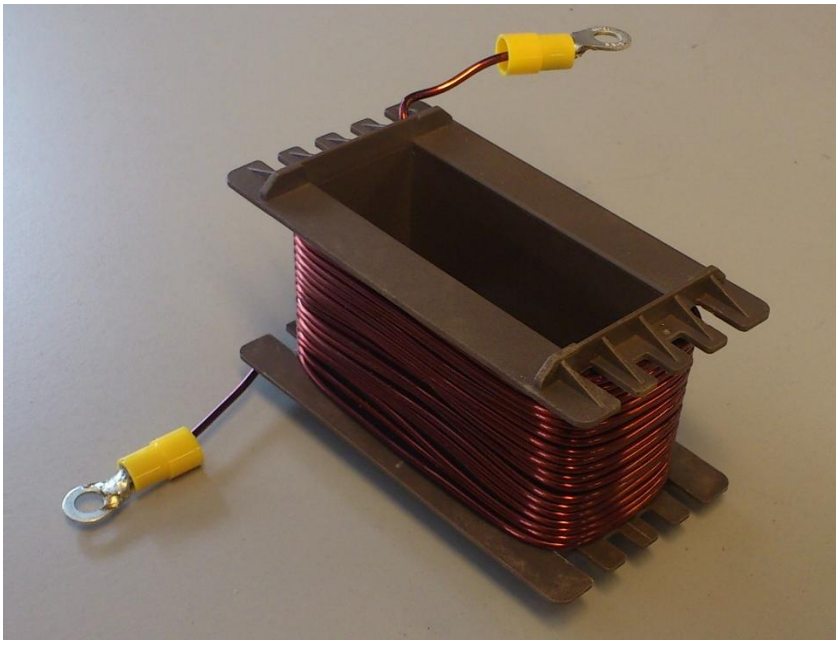

Figure 37 - Resonant tank inductor for the lab setup

The IGBT bridge is shown in Figure 38. It consists of four 1200 V/40 A IGBT's without antiparallel diodes, which were added later to the setup. The components were placed on a heat sink to enhance heat dissipation. To avoid generating parasitic inductance that would alter the frequency characteristic of the circuit, flat copper busbars were used to connect the components together. To prevent accidental short circuits or touching live conductors, most of the busbars were insulated with the insulation removed only at the points where contacts were soldered.

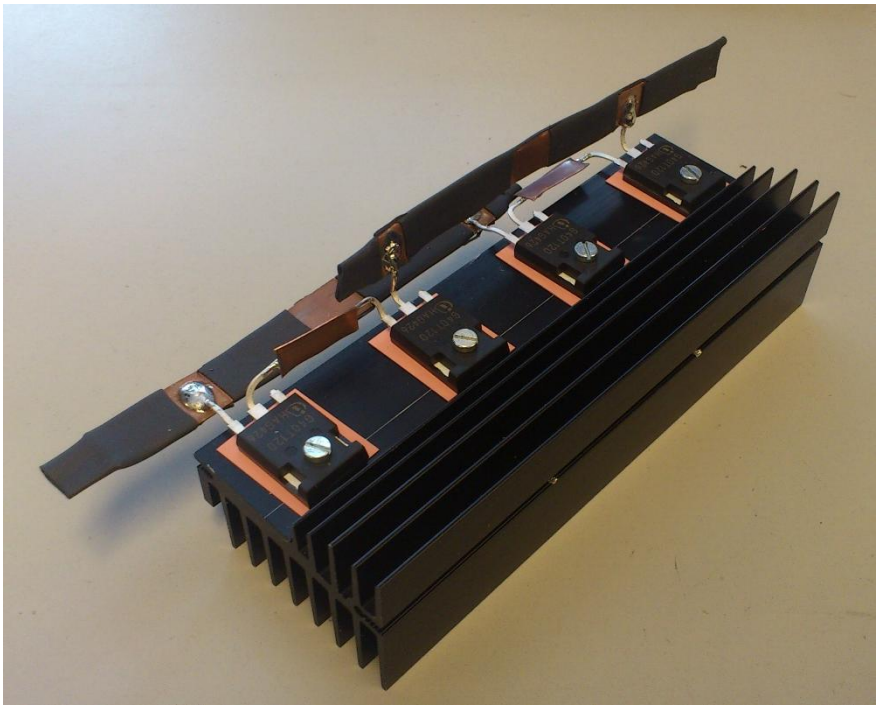

Figure 38 - IGBT bridge for the lab setup

The IGBT bridge was driven by a pair of single-input, isolated high/low side gate drivers. Each driver had an integrated dead time and overlap protection, giving mutually inverse pulses to both the high and low side transistors within one converter leg. This is more closely shown in Figure 39. The other converter leg used the same gate driver model, but with high and low side gate pulses inverted. This configuration made controlling the full bridge converter using only a single signal generator possible. The complete driver circuit configuration was implemented on a stripboard, together with capacitors for stabilizing the terminal supply voltages, dead time control resistor and a bootstrap circuit.

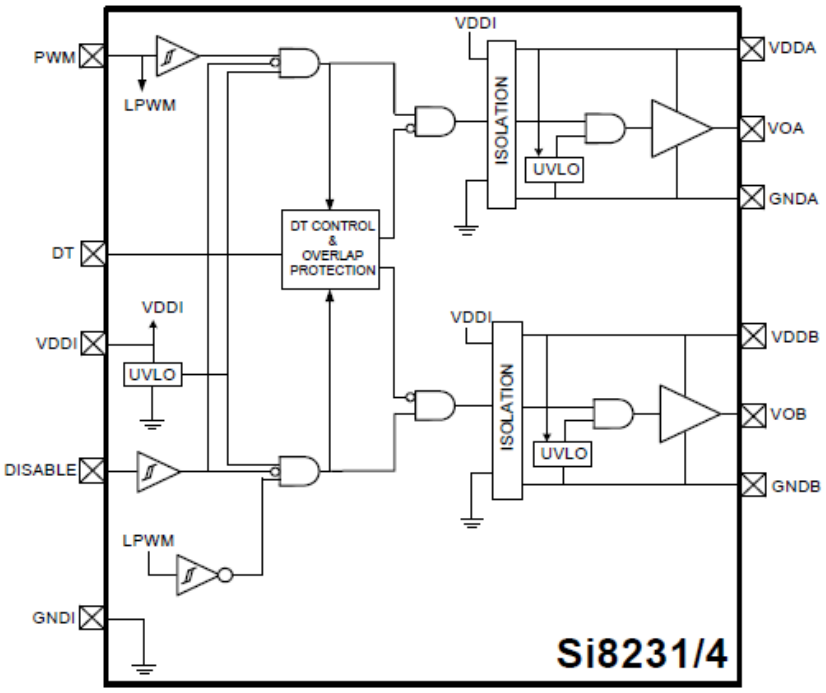

Figure 39 - Internal gate driver module configuration [11]

Gate driver circuit test is shown in Figure 40. Control signal comes from the signal generator and has an amplitude between 0 - 5 V. Output side of the gate driver is supplied from a 15 V source, which is also the voltage used to turn the transistors on. The top and bottom gate signals are mutually inverse and stable, which validates the circuit operation.

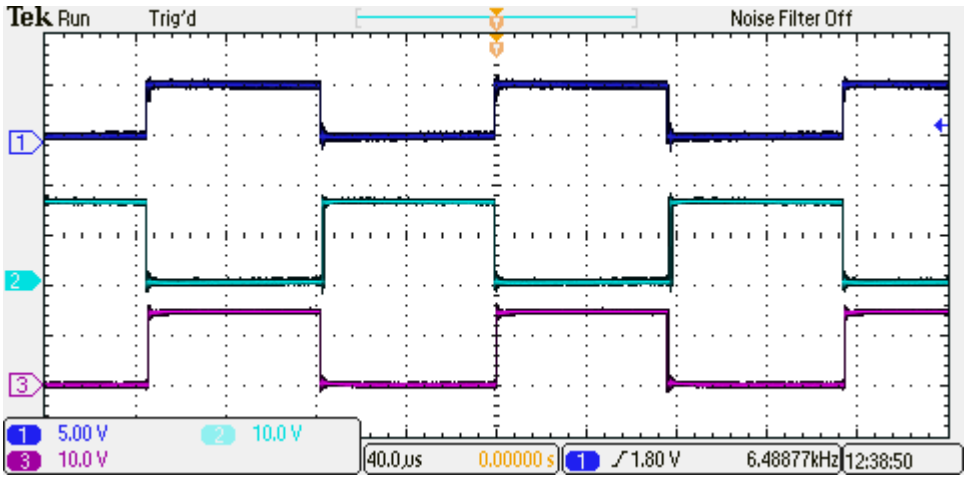

Figure 40 - Gate driver circuit test: gate control signal (1), bottom gate voltage (2), top gate voltage (3)

To avoid short circuiting the input voltage source, dead time had to be implemented to make sure one transistor has enough time to turn off before the other one turns on. From the device datasheet [12] it was obtained that the highest switching time occurs at a turn-off

at zero current and equals 800 ns. Dead time was programmed by connecting a resistor between the gate driver's DT pin and the supply voltage ground and its magnitude had been selected to give dead time of 1 µs. Dead time test is shown in Figure 41, which confirms it had been programmed correctly.

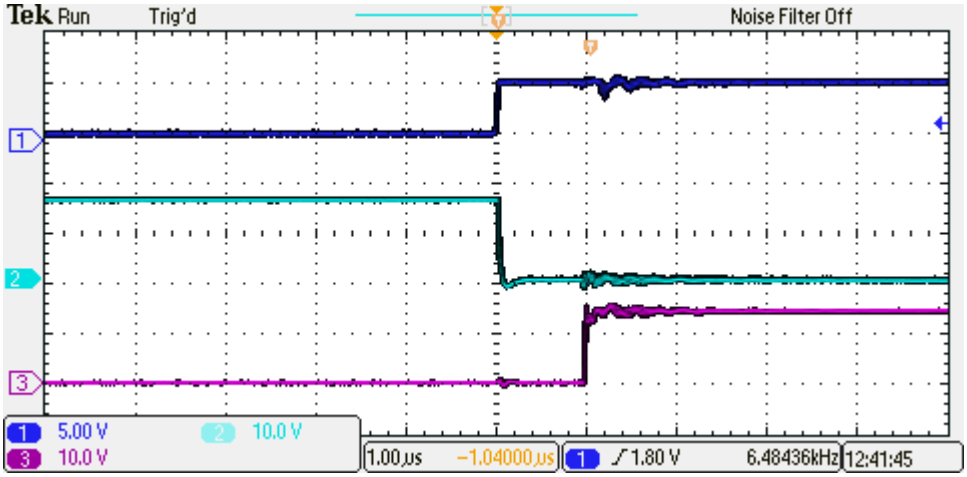

Figure 41 - Dead time test: gate control signal (1), bottom gate voltage (2), top gate voltage (3)

As shown earlier, dead time can in some cases seriously influence the converter circuit's performance. In this particular case, the highest frequency IGBTs would operate at during normal operation is half of the resonant frequency, giving a time period of 162 µs. This results in duty cycle of the gate signal of 99.3 %, which should not have any unwanted impacts on the circuit's performance according to the findings of section 4.2.5.

The rectifier bridge is shown in Figure 42. As the IGBT converter, it was also attached to a heat sink and connected using insulated copper busbars. It consists of four 300 V/2x15 A fast recovery diodes. Since the anodes have been shorted, the maximum current each device can withstand is 30 A.

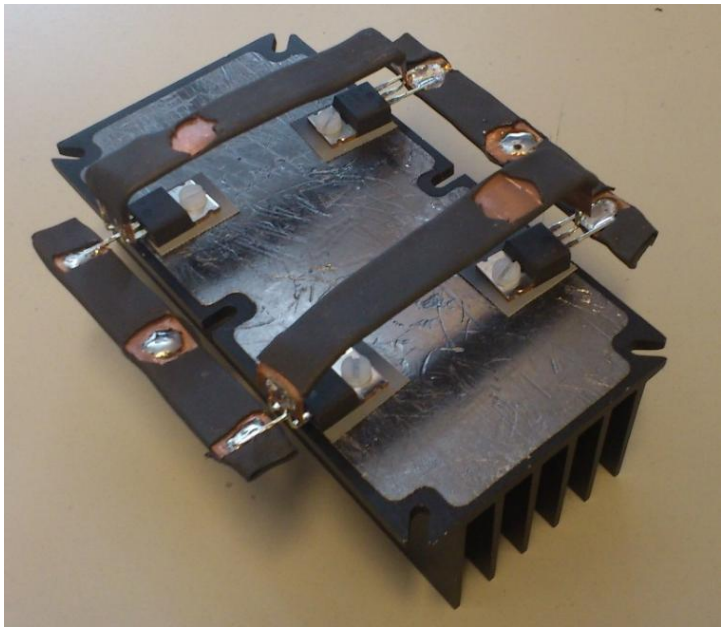

Figure 42 - Diode rectifier bridge for the lab setup

The transformer and resonant tank parameters are given in Table 2. The same parameters were used in the loss estimation simulation.

Table 2 – Transformer and resonant tank parameters measured at 10 kHz

Parameter	Description	Value
L_m	Transformer magnetization inductance	933 µH
L_l	Transformer leakage inductance	8.7 µH
R_T	Transformer winding resistance	238 mΩ
N_1	Number of turns on the primary	7
N_2	Number of turns on the secondary	18
L	Air core inductor's inductance	19.1 µH
R_L	Air core inductor's series resistance	100 mΩ
C	Resonant tank capacitor's capacitance	6 µF
R_c	Resonant tank capacitor's series resistance	108 mΩ

Having all of the key circuit parameters measured, it is possible to finalize the design and give the preliminary converter specification in Table 3.

Table 3 - Preliminary converter specification for the lab setup

Parameter	Value
Power rating	150 W
Nominal input voltage	40 V
Input voltage tolerance	± 10%
Nominal output voltage	40 V
Output voltage tolerance	± 10%
Resonant frequency	12.32 kHz

The power rating was calculated using (46). Since this power relation was derived for a lossless circuit, the actual maximum power output achievable within the given voltage limits while staying in DCM is lower. This means that, in case both the output and input voltages drop 10% from their nominal value at the same time, the converter will have to enter CCM to continue delivering 150 W at its output.

6.2 Simulation results

The laboratory circuit was modelled in Plecs and used to estimate conduction and switching losses. I-V curves for calculating the conduction losses of semiconductor devices were obtained from the component datasheets [12], [13], [14], together with E-I curves for the IGBT turn-on and turn-off power loss estimation. The rectifier diode datasheet did not contain such a table, so the switching losses in the passive rectifier were neglected. However, since turn-offs and turn-ons always occur at zero current, it is safe to assume the majority of losses associated with the rectifier will be caused by conduction rather than switching.

The losses were evaluated at different operating points. Figure 14 shows how the losses change with the output power. The output power was varied from 10 to 110% of its nominal value, while the input and output voltages were kept constant at 40 V. Due to the fact all the switching occurs at zero current, the estimated switching losses were below 20 mW and therefore omitted from the figure.

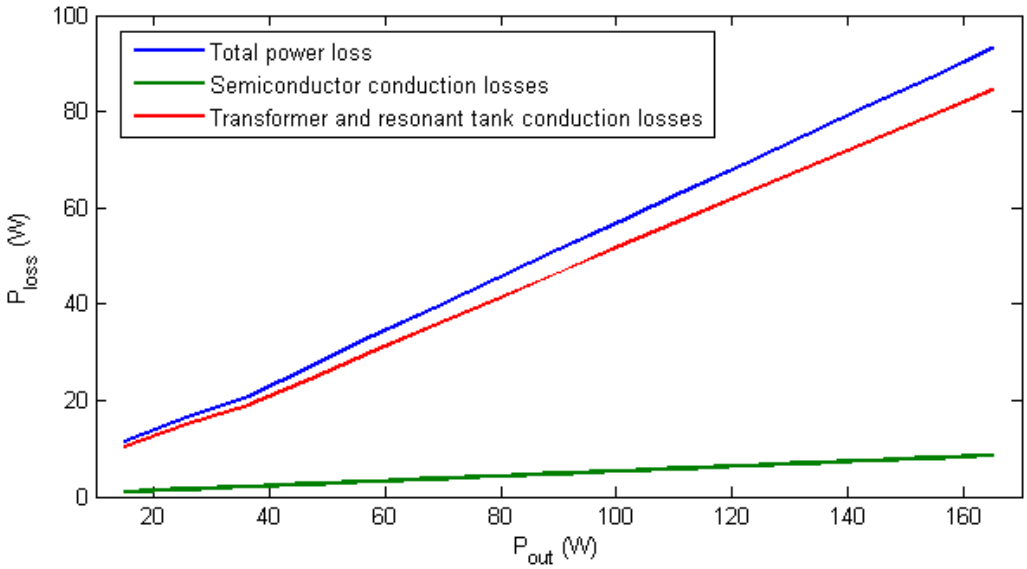

Figure 43 - Power loss dependence on output power at nominal voltage level

Two important things are visible from the graph. First, the relationship between the power loss and the output power is linear within the whole operating range, even though it has been shown in (53)-(55) that the conduction losses in semiconductors are nonlinear, while the conduction losses in copper are proportional to the current squared. This is due to the fact the converter can deliver 110% of output power at nominal voltage while remaining in DCM.

As discussed earlier, current and voltage waveforms in DCM stay the same while the converter is conducting, resulting in the same amount of energy transferred each switching period. Since the peak, average and RMS current values do not change over the conducting part of the switching period, the conduction losses they generate also stay the same. On the other hand, since there is no conduction during the remainder of the switching period, there are no conduction losses either. Maintaining constant efficiency over the full operating range is therefore an inherent property of DCM resonant converters. This is not the case with converters operating in CCM where the current amplitude changes together with the power reference.

The second visible property is very poor efficiency of only 64% due to excessively high copper losses. One of the reasons for that is an additional inductor wounded to increase the transformer's leakage inductance, increasing the wire length and thus series resistance of the circuit. Another reason is that the transformer and air-core inductor were, due to lack of materials in the lab, wounded using solid copper wire. At the current frequency of 12.32 kHz, this lead to an increase of 21% in the effective AC resistance due to skin effect compared to wire's DC resistance. This means that copper losses would have been 17.4% lower if stranded wire was used to wind the transformer and the inductor. Further improvements could be achieved by using conductors specially designed for higher frequencies, such as Litz wire.

Figure 44 shows how the total losses change for different input and output voltages. The worst operating point is located at the maximum input and minimum output voltage. This is caused by the fact the highest DC voltage ratio also results in highest peak current, which in return causes the highest conduction losses. On the other hand, the operating point with the lowest losses is located at the lowest DC voltage ratio. At this point the circuit is operating in CCM, which leads to a reduction of peak-to-RMS current ratio and in this case, peak current value in general, reducing the conduction losses.

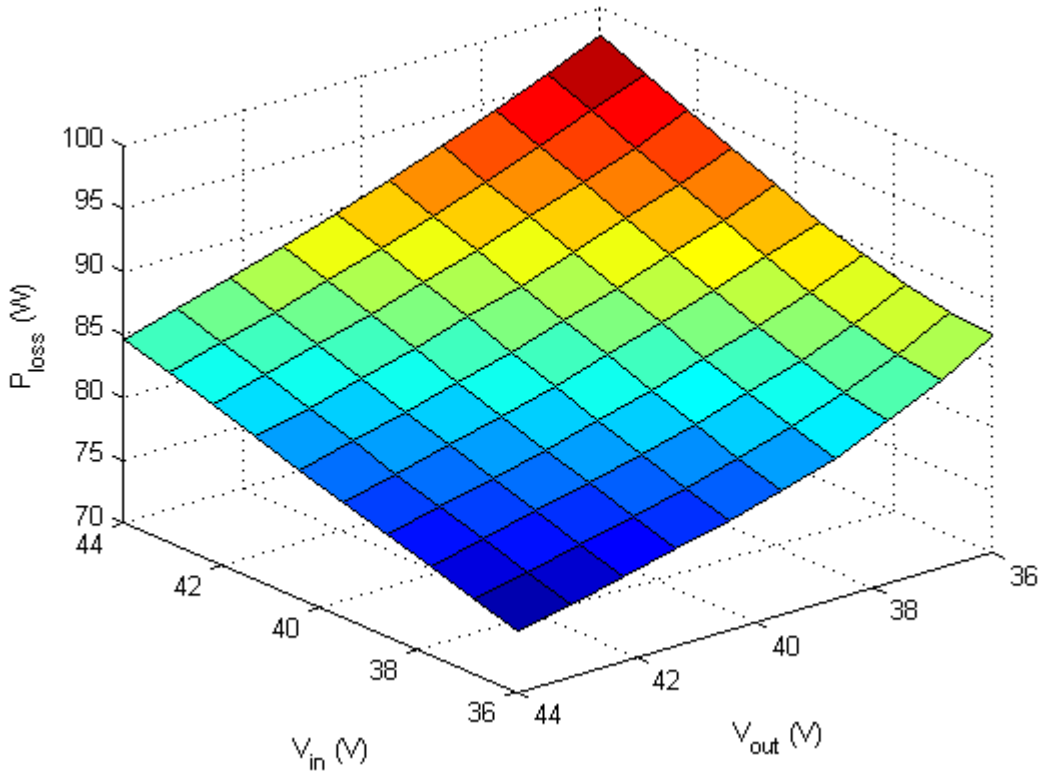

Figure 44 - Power loss dependence on input and output voltages at full power

At the same time, IGBTs do not switch at zero current anymore, increasing the switching losses to 0.2 W, which is around 10x higher than when the circuit operated in DCM. However, due to the fact the switching current is only 10% of its peak value, as well as the fact copper losses are dominant in this circuit, the reduction in conduction losses weights out the increase in switching losses. This is thus also the optimal operating point where the converter achieves highest efficiency as no particular demands were made that the converter should operate in DCM at all times, or the capacitor voltage should be limited to a certain value.

Figure 45 is closely related to the previous one and shows how the converter efficiency changes throughout the same operating points. The highest efficiency converter achieves in the given operating range is 0.667, while the lowest 0.606.

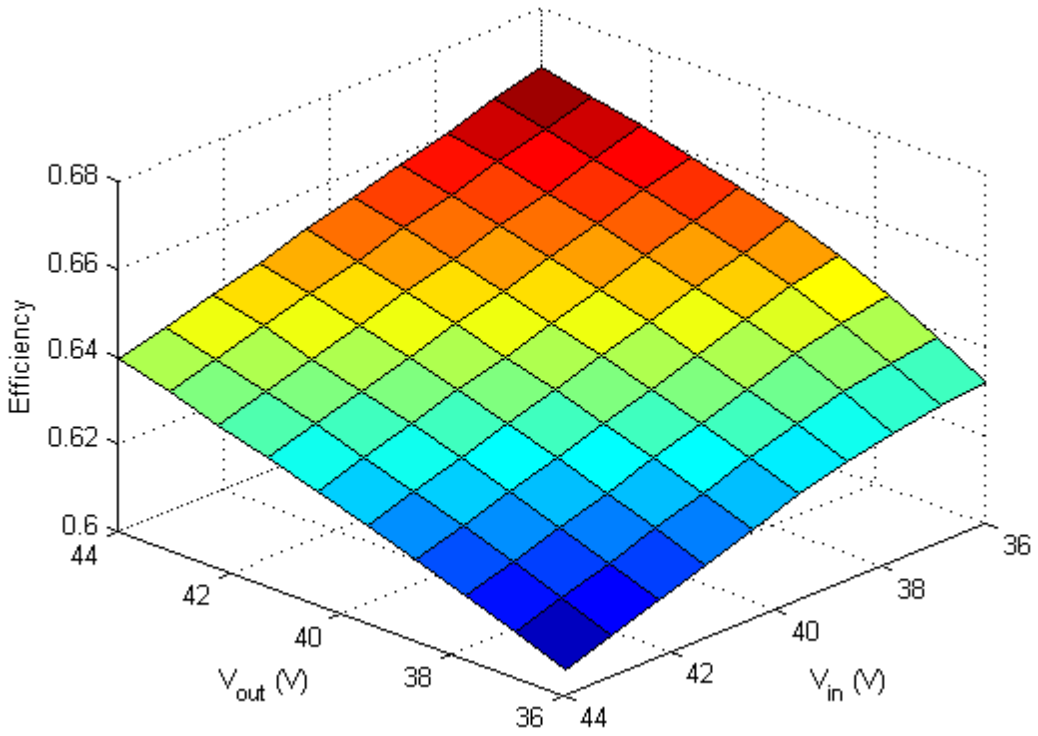

Figure 45 - Efficiency dependence on input and output voltages at full power

The simulation results show that, for small-size, low-power converters, the design should be oriented towards reducing the conduction losses, meaning that the converters should operate in CCM. Thin conductors lead to high characteristic resistance of the circuit, which is even more emphasized in this particular case since the skin effect had not been taken care of. Moreover, due to relatively low current and voltage levels used, it is fairly easy and cheap to acquire oversized components and therefore minimize the risk of their overload. This rendered another beneficial property of DCM – relatively low capacitor voltage – useless.

On the other hand, for high power circuits, including the 10 MW proposal made, it might be completely infeasible to allow the peak capacitor voltage to become several dozens of times higher than the already high input voltage. High currents on the other hand not only impose limitations on transistors in the form of maximum current they can switch at, but also significantly increase the switching losses. On the other hand, increase in dimensions typically reduces the circuit's resistance and consequently characteristic conduction losses. This means that, at high power, the switching losses might constitute a dominant portion of the circuit's losses, therefore making DCM a much more feasible solution, both from the efficiency and component rating viewpoint.

6.3 Experimental results

By the time of finishing this report, the converter circuit had been built, but not fully operational due to certain issues with antiparallel diodes which caused input voltage instability when entering DCM. The issues were most probably caused by parasitics in the cables used to connect diodes to IGBTs. Due to the limited timeframe and lack of readily available components, it had not possible to obtain new components and rebuild the IGBT bridge before the thesis submission date. As a result, it was possible to obtain voltage and current waveforms from the setup and compare them to the ones obtained by simulation, but not possible to evaluate the loss estimation from the previous section as the circuit had not been operating in the same conditions as in the simulation. Furthermore, since the circuit was not fully operational, the input and output voltages were limited to ± 10 V to avoid damaging the test setup or the equipment due to a fault.

The parasitics also caused the assembled test circuit to change some of its parameters compared to those obtained by measuring each component separately. This namely effected the circuit's resonant frequency, which was measured to be 14.13 kHz. The resonance point operation is shown in Figure 46.

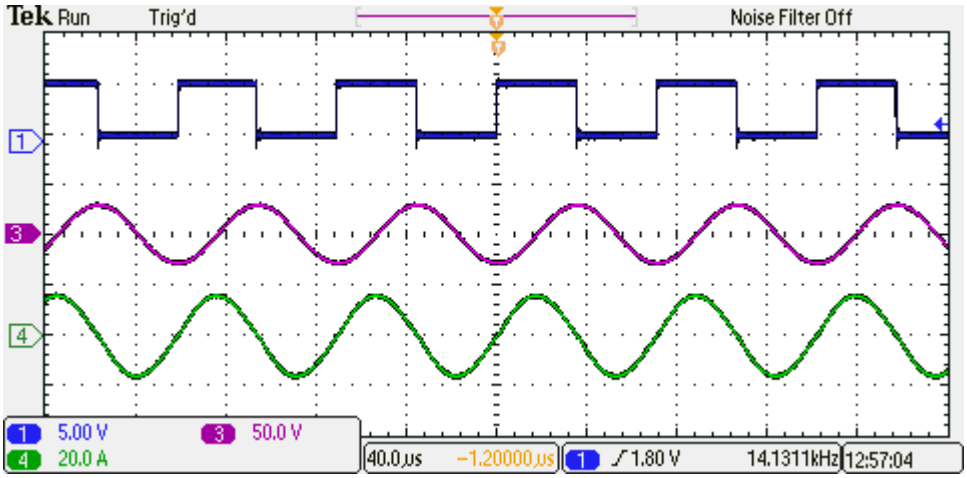

Figure 46 - Test setup waveforms at resonant frequency: gate control signal (1), capacitor voltage (3), inductor current (4)

At the resonance frequency, the peak capacitor voltage is 32 V, while the inductor current peaks at 16 A. The current, and consequently the capacitor voltage, are in this case limited by the circuit's series resistance. The simulation results for the resonant frequency of

the simulation circuit with old parameters is shown in Figure 47. The peak capacitor voltage equals 37.6 V, while the peak inductor current 17.5 A. The results are fairly close to measured values, which implies that the differences between the simulated and actual circuit are caused by parasitic properties of wires and connectors used to connect the components together. The wires connecting the components clearly increased the circuit's series resistance, while the frequency response could have been influenced by several factors, such as relative placement of the components, wires and connectors itself or the addition of DC link capacitors for voltage stabilization.

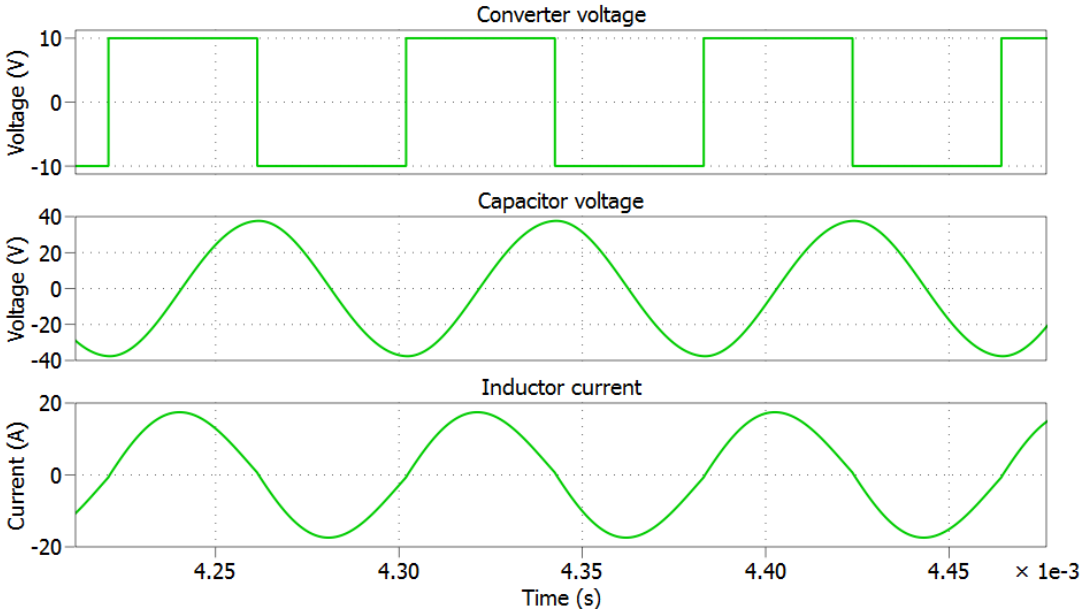

Figure 47 - Simulation results for test circuit with original parameters at resonant frequency

Measurements performed at resonant frequency confirmed the findings from section 4.2.2 stating that the highest component stress occurs at resonant frequency. However, due to the circuit's low quality factor, capacitor voltage peaked at only 3.2 times the input voltage. Inductor current on the other hand reached fairly high values, drawing more than 100 W of power from the 10 V input source.

Discontinuous conduction mode waveforms are shown in Figure 48. The figure depicts filtered waveforms as the actual results had a lot of noise due to earlier stated problem with the setup. Even so, obtained waveforms clearly reflect the waveforms obtained by simulations from section 4.3, thus validating the principal model of series-resonant converter used.

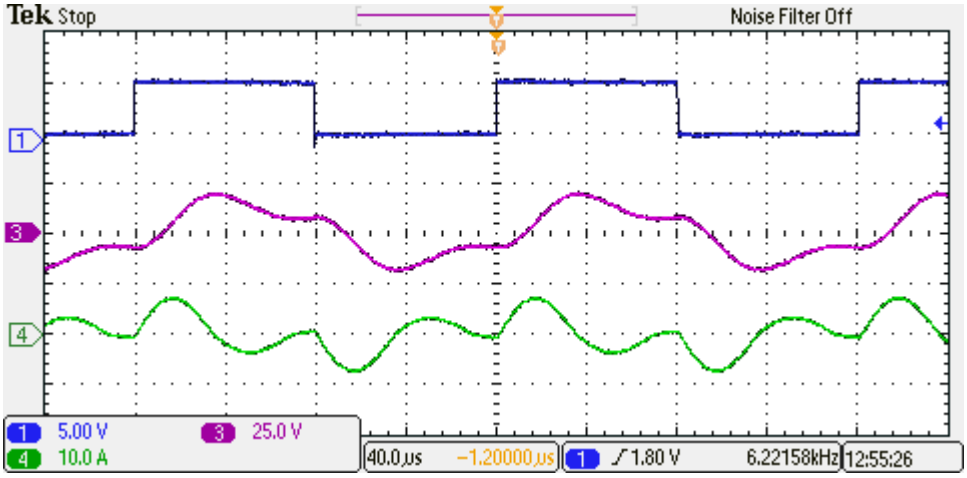

Figure 48 - Test setup waveforms in DCM: gate control signal (1), capacitor voltage (3), inductor current (4)

The measurements confirm two biggest advantages of DCM. Peak capacitor voltage equals 20 V, thus confirming relation (30) about the capacitor voltage being limited to twice the input voltage in DCM. Comparing the inductor current waveform with the gate control signal on the other hand confirms that both the IGBTs and diodes turn on and off at zero current and therefore have minimal switching losses.

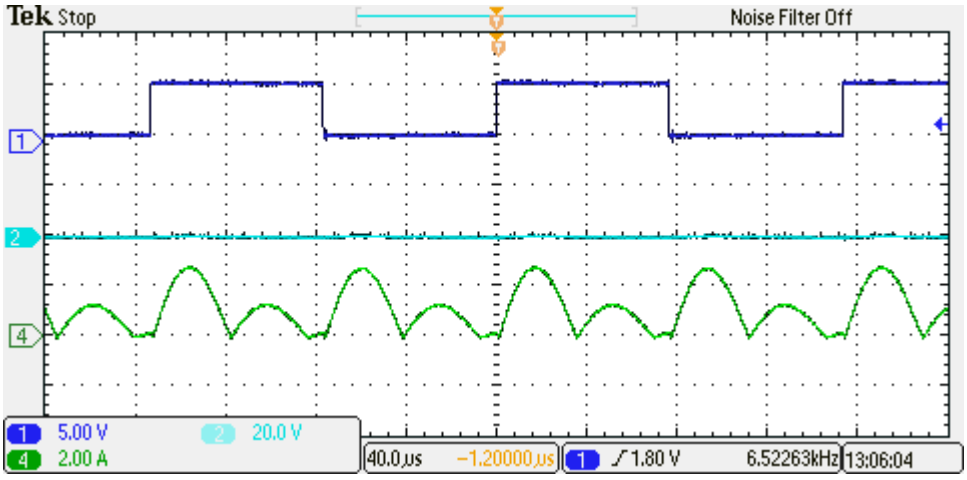

Figure 49 - Test setup waveforms in DCM: gate control signal (1), output current (4)

The output current waveform in DCM is shown in Figure 49. The second input is unused. Once again, the waveforms coincide well with the ones obtained by simulation. The output current equals the rectified inductor current scaled by the transformer's transfer ratio. The measurements confirm another statement from section 4.3 stating that peak-to-average ratio of the output current in DCM is higher than in CCM.

Most important points stated in this chapter are the following:

- Two important things that should be taken into account when building a real SRC circuit are transformer saturation and the amount of dead time added
- The laboratory circuit had excessive conduction losses due to skin effect and unnecessarily high wire length, which is why stranded wire should be used to wind and connect the components while the resonant tank inductor should be included in the transformer's leakage inductance
- DCM converters maintain constant efficiency over the whole operating range for stable input and output voltages
- CCM is a better choice for low power circuits as they typically have high conduction and low switching losses with only few or no device limitations
- DCM is a better candidate for high power circuits due to device limitations, higher characteristic switching losses and lower characteristic conduction losses compared to low power circuits
- Experimental results have validated several statements from section 4, such as that peak component stress occurs at resonant frequency, DCM limits the peak capacitor voltage to twice the input voltage, IGBTs and diodes switch at zero current in DCM and peak-to-average value of output current is higher in DCM than in CCM

7 Conclusion

This report contains the analysis, design procedure, simulation results and a lab setup description of a series-resonant DC/DC converter circuit.

The converter circuit, even though inherently nonlinear, can be modelled using a set of 3 equivalent linear circuits containing ideal voltage and current sources when the switching frequency is close to the resonant frequency of the resonant tank.

The steady-state analysis has shown how the circuit responds to a change of input and output voltages, switching frequency, duty cycle and resonant tank's inductance and capacitance. The biggest problems identified were high voltage and current stress on the resonant tank components and the circuit's nonlinear responsiveness the change of switching frequency. A separate analysis was performed for the discontinuous conduction mode, which reduces the component voltage stress and switching losses, but in return leads to increased conduction losses. Power relations have been derived for both conduction modes and revealed that another benefit of DCM is a linear relationship between the switching frequency and the output power.

Based on the analysis' results, general guidelines for series-resonant converter design have been derived and used to make a 10 MW circuit proposal and its corresponding control system. To analyze the characteristic losses of the converter, a 150 W lab prototype was built and based on the measured parameters and component datasheets, the losses were estimated in a Plecs simulation. The simulation revealed that the designed circuit had not been optimized for higher frequencies and therefore had excessive copper losses.

Due to the limited timeframe and lack of readily available components, the lab setup had not been fully operational before the project submission date and therefore a comparison between the simulated and measured waveforms at full power has not been made. However, measurements performed at reduced voltage levels have shown that voltage and current waveforms of a test setup reflect the ones obtained by simulations. Main advantages of discontinuous conduction mode – limited capacitor voltage and zero current switching have also been experimentally validated.

Overall conclusion drawn from building the lab setup is that for converters of low size and power, continuous conduction mode should be used as the conduction losses constitute a dominant portion of the total power loss. For high power converters on the other hand, device limitations and an increased share of switching losses make discontinuous conduction mode a better candidate.

8 List of abbreviations

AC	Alternating Current
CCM	Continuous Conduction Mode
CD	Compact Disc
DC	Direct Current
DCM	Discontinuous Conduction Mode
DT	Dead Time
GUI	Graphical User Interface
HV	High Voltage
IGBT	Insulated Gate Bipolar Transistor
LV	Low Voltage
MF	Medium Frequency
MV	Medium Voltage
PI	Proportional Integral
PWM	Pulse Width Modulation
RMS	Root Mean Square
SRC	Series-Resonant Converter

9 References

[1] Fraunhofer ISE, Levelized Cost of Electricity: Renewable Energy Technologies, Freiburg, Germany, 2013.

[2] R. Erickson and D. Maksimovic, Fundamentals of Power Electronics, Boulder, Colorado: Kluwer Academic, 1997.

[3] N. Mohan, T. M. Undeland and W. P. Robbins, Power Electronics: Converters, Applications and Design, John Wiley & Sons, Inc., 2002.

[4] D. Graovac and M. Purschel, "IGBT Power Losses Calculation Using the Data-Sheet Parameters," Infineon Technologies AG, Neubiberg, Germany, 2009.

[5] U. Drofenik and J. W. Kolar, "A General Scheme for Calculating Switching- and Conduction-Losses of Power Semiconductors in Numerical Circuit Simulations of Power Electronic Systems," in *International Power Electronics Conference*, Niigata, Japan, 2005.

[6] A. D. Rajapakse, A. M. Gole and P. L. Wilson, "Approximate Loss Formulae for Estimation of IGBT Switching Losses through EMTP-type Simulations," in *6th International Conference of Power System Transients*, 2005.

[7] N. Soltau, D. Eggers, K. Hameyer and R. W. D. Doncker, "Iron Losses in a Medium-Frequency Transformer Operated in a High-Power DC-DC Converter," *IEEE Transactions on Magnetics,* vol. 50, no. 2, 2014.

[8] I. Villar, I. Etxeberria-Otadui, U. Viscarret and A. Rufer, "Global Loss Evaluation Methods for Nonsinusoidally Fed Medium-Frequency Power Transformers," *IEEE Transactions on Industrial Electronics,* vol. 56, no. 10, pp. 4132-4140, 2009.

[9] G. Ortiz, M. Leibl, J. W. Kolar and O. Apeldoorn, "Medium Frequency Transformers for Solid-State Applications: Design and Experimental Verification," in *IEEE 10th International Conference on Power Electronics and Drive Systems*, 2013.

[10] TDK, "Ferrites and accessories - SIFERRIT material N87," 2006.

[11] Silicon Labs, "0.5 and 4.0 Amp ISOdrivers Si823x," Silicon Laboratories Inc., Austin, Texas.

[12] Infineon, "IGW40T120 datasheet," Infineon Technologies AG, München, Germany, 2009.

[13] Vishay, "VS-30CTH03-N3 datasheet," Vishay Semiconductors, 2012.

[14] Vishay, "VS-80EBU02 datasheet," Vishay Semiconductors, 2012.

[15] P. A. J. V. Rensburg and H. C. Ferreira, "The Role of Magnetizing and Leakage Inductance in Transformer Coupling Circuitry," in *8th ISPLC*, Zaragoza, Spain, 2004.

[16] R. Nielsen, "LLC and LCC resonance converters: Properties, Analysis, Control," Tommerup, Denmark, 2013.

10 Appendix

The CD handed in alongside this report contains the following:

- Series-resonant converter analysis tool with GUI
- Full plot catalogue from section 4.2
- Plecs models of 150 W and 10 MW circuit
- Lab component datasheets
- This report in PDF